Jamming of soft particles: geometry, mechanics, scaling and isostaticity

2010 J. Phys.: Condens. Matter 22 033101

(http://iopscience.iop.org/0953-8984/22/3/033101)

IOP Publishing Journal of Physics: Condensed Matter

J. Phys.: Condens. Matter **22** (2010) 033101 (24pp) doi:10.1088/0953-8984/22/3/033101

TOPICAL REVIEW

Jamming of soft particles: geometry, mechanics, scaling and isostaticity

M van Hecke

Kamerlingh Onnes Laboratory, Leiden University, PO Box 9504, 2300 RA Leiden, The Netherlands

E-mail: mvhecke@physics.leidenuniv.nl

Received 20 July 2009, in final form 10 November 2009
Published 16 December 2009
Online at stacks.iop.org/JPhysCM/22/033101

Abstract

Amorphous materials as diverse as foams, emulsions, colloidal suspensions and granular media can *jam* into a rigid, disordered state where they withstand finite shear stresses before yielding. Here we review the current understanding of the transition to jamming and the nature of the jammed state for disordered packings of particles that act through repulsive contact interactions and are at zero temperature and zero shear stress. We first discuss the breakdown of affine assumptions that underlies the rich mechanics near jamming. We then extensively discuss jamming of frictionless soft spheres. At the jamming point, these systems are marginally stable (isostatic) in the sense of constraint counting, and many geometric and mechanical properties scale with distance to this jamming point. Finally, we discuss current explorations of jamming of frictional and non-spherical (ellipsoidal) particles. Both friction and asphericity tune the contact number at jamming away from the isostatic limit, but in opposite directions. This allows one to disentangle the distance to jamming and the distance to isostaticity. The picture that emerges is that most quantities are governed by the contact number and scale with the distance to isostaticity, while the contact number itself scales with the distance to jamming.

(Some figures in this article are in colour only in the electronic version)

Contents

1. Introduction

Jamming governs the transition to rigidity of disordered matter. Foams, emulsions, colloidal suspensions, pastes, granular

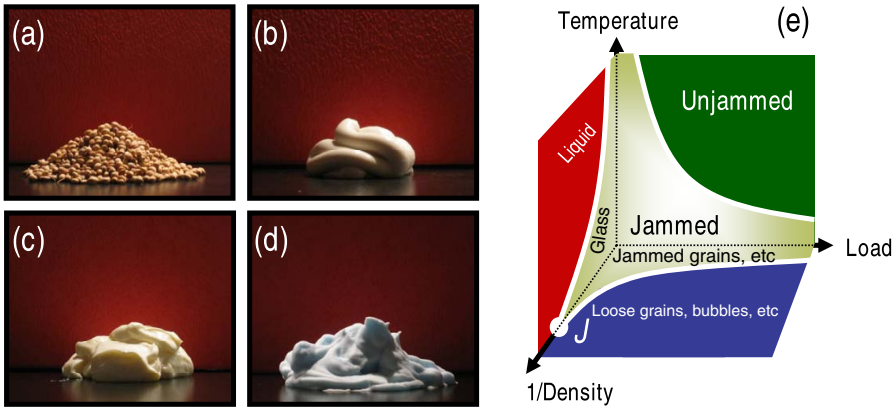

Figure 1. (a)–(d) Examples of everyday disordered media in a jammed state. (a) Granular media, consisting of solid grains in gas or vacuum. (b) Toothpaste, a dense packing of (colloidal) particles in fluid. (c) Mayonnaise, an emulsion consisting of a dense packing of (oil) droplets in an immiscible fluid. (d) Shaving foam, a dense packing of gas bubbles in fluid. (e) Jamming diagram proposed by Liu *et al* [1, 2]. The diagram illustrates that many disordered materials are in a jammed state for low temperature, low load and large density, but can yield and become unjammed when these parameters are varied. In this review we will focus on the zero-temperature, zero-load axis. For frictionless soft spheres, there is a well-defined jamming transition indicated by point 'J' on the inverse density axis, which exhibits similarities to an (unusual) critical phase transition.

media and glasses can *jam* in rigid, disordered states in which they respond essentially elastically to small applied shear stresses (figures 1(a)–(d)). However, they can also easily be made to yield (unjam) and flow by tuning various control parameters.

The transition from the freely flowing to the jammed state, the jamming transition, can be induced by varying thermodynamic variables, such as temperature or density, but also mechanical variables such as the stress applied to the sample: colloidal suspensions become colloidal glasses as the density is increased near random close packing, flowing foams become static as the shear stress is decreased below the yield stress, and supercooled liquids form glasses as the temperature is lowered below the glass transition temperature. In 1998 Liu and Nagel presented their provocative jamming phase diagram (figure 1(e)) and proposed to probe the connections between various transitions to rigidity [1].

This review provides an overview of the current (partial) answers to the following two questions: what is the nature of the jammed state? What is the nature of the jamming transition? We focus on jammed model systems at zero temperature and zero shear—models for non-Brownian emulsions, foams and granular media rather than colloidal and molecular glasses—and review the geometrical and mechanical properties of these systems as a function of the distance to jamming.

In view of the very rapid developments in the field, this paper focuses on the basic jamming scenarios, which arise in (weakly) compressed systems of soft particles interacting through repulsive contact forces at zero temperature and zero shear. The picture that has emerged for the jamming transition in these systems is sufficiently complete to warrant an overview article and, in addition, provides a starting point for work on a wider range of phenomena, such as occurring in attractive systems [3], systems below jamming [4], the flow of disordered media near jamming [5–9], jamming of systems at finite temperature [10, 11] and experiments [12–14].

In this review the focus is on jamming of frictionless spheres, frictional spheres and frictionless ellipsoids—soft (deformable) particles which interact through repulsive contact forces. The distance to jamming of all these systems is set by the amount of deformation of the particles, which can be controlled by the applied pressure or enforced packing fraction. These systems lose rigidity when the deformations vanish or, equivalently, when the confining pressure reaches zero. As we will see, these seemingly simple systems exhibit rich and beautiful behavior, where geometry and mechanical response are intricately linked.

The contact number, z, defined as the average number of contacts per particle, plays a crucial role for these systems. There is a minimal value of z below which the system loses rigidity: when the contact number is too small, there are collective particle motions, so-called floppy modes, that (in lowest order) do not cost elastic energy. By a constraint counting argument one can establish a precise value for the minimum value of z where the system does not generically allow floppy deformations—this is the isostatic contact number $z_{\rm iso}$. As we will see, a host of mechanical and geometrical properties of jammed systems scale with distance to the isostatic point.

The crucial, and at first glance very puzzling, point is that, while frictionless spheres reach isostaticity at the jamming point, frictional spheres are generally hyperstatic ($z > z_{\rm iso}$) at jamming, while frictionless ellipsoids are hypostatic ($z < z_{\rm iso}$) at jamming. As we will see, the relations between contact numbers, floppy modes, rigidity and jamming are subtle.

Truly new and surprising physics emerges near jamming in systems as seemingly simple as disordered packings of frictionless, deformable particles [2]. We first discuss the breakdown of affine assumptions that underlies the rich physics of jamming in section 2. We give an overview of the main characteristics of the jamming transition for soft frictionless spheres in section 3. Both friction and asphericity lead to new physics, as here the jamming transition and isostaticity

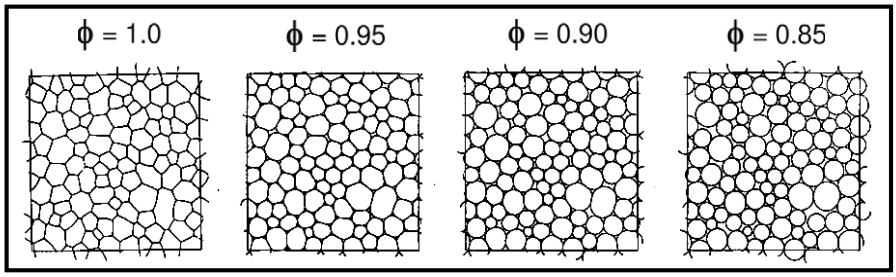

Figure 2. Simulated foam for increasing wetness, approaching unjamming for $\phi \downarrow 0.84$ (adapted from [15] with permission—copyright by the American Physical Society).

decouple. Jamming of frictional soft spheres is discussed in section 4 and jamming of frictionless soft ellipsoids in section 5. Finally, in section 6 we sketch a number of open problems.

2. Motivation: mechanics of disordered matter

The crucial question one faces when attempting to describe the mechanics of materials such as foams, emulsions or granular media, is how to deal with disorder. The simplest approach is to ignore disorder altogether and attempt to gain insight based on models for ordered, 'crystalline' packings. A related approach, effective medium theory, does not strictly require ordered packings, but assumes that local deformations and forces scale similarly as global deformations and stresses. As we will see in section 2.1, major discrepancies arise when these approaches are confronted with (numerical) experiments on disordered systems. This is because the response of disordered packings becomes increasingly non-affine near jamming (section 2.2).

2.1. Failure of affine approaches

2.1.1. Foams and emulsions. Some of the earliest studies that consider the question of the rigidity of packings of particles concern the loss of rigidity in foams and emulsions with increasing wetness. Foams are dispersions of gas bubbles in liquid, stabilized by surfactant, and the gas fraction ϕ plays a crucial role for the structure and rigidity of a foam. The interactions between bubbles are repulsive and viscous, and static foams are similar to the frictionless soft spheres discussed in section 3. In real foams, gravity (which causes drainage) and gas diffusion (which causes coarsening) play a role, but we will ignore these.

The unjamming scenario for foams is as follows. When the gas fraction approaches 1, the foam is called dry. Application of deformations causes the liquid films to be stretched, and the increase in surface area then provides a restoring force: dry foams are jammed. When the gas fraction is lowered and the foam becomes wetter, the gas bubbles become increasingly spherical, and the foam loses rigidity for some critical gas fraction ϕ_c where the bubbles lose contact (figure 2). The unjamming transition is thus governed by the gas fraction, which typically is seen as a material parameter. For emulsions, consisting of droplets of one fluid dispersed in a second fluid and stabilized by a surfactant, the same scenario arises.

Analytical calculations are feasible for ordered packings, because one only needs to consider a single particle and its neighbors to capture the packing geometry and mechanical response of the foam—due to the periodic nature of the packing, the response of the material is affine. The affine assumption basically states that, locally, particles follow the globally applied deformation field—as if the particles are pinned to an elastically deforming sheet. More precisely, the strict definition of affine transformations states that three collinear particles remain collinear and that the ratio of their distances is preserved and affine transformations are, apart from rotations and translations, composed of uniform shear and compression or dilatation.

Packings of monodisperse bubbles in a two-dimensional hexagonal lattice ('liquid honeycomb' [16]) deform affinely. The bubbles lose contact at the critical density ϕ_c equal to $\frac{\pi}{2\sqrt{3}} \approx 0.9069$ and ordered foam packings are jammed for larger densities [16, 17]. When for such a model foam ϕ is lowered towards ϕ_c, the yield stress and shear modulus remain finite and jump to zero precisely at ϕ_c [16, 17]. The contact number (average number of contacting neighbors per bubble) remains constant at 6 in the jammed regime. Similar results can be obtained for three-dimensional ordered foams, where ϕ_c is given by the packing density of the HCP lattice $\frac{\pi}{3\sqrt{2}} \approx 0.7405$.

Early measurements for polydisperse emulsions by Princen and Kiss in 1985 [18] found a shear modulus which varied substantially with ϕ. Even though no data was presented for ϕ less than 0.75 and the fit only included points for which $\phi \geqslant 0.8$, the shear modulus was fitted as $G \sim \phi^{1/3}(\phi - \phi_c)$, where $\phi_c \approx 0.71$, and thus appeared to vanish at a critical density below the value predicted for ordered lattices [18].

The fact that the critical packing density for ordered systems is higher than that for disordered systems may not be a surprise, given that, at the jamming threshold, the particles are undeformed spheres and it is well known that ordered sphere packings are denser than irregular ones [19]. However, the differences between the variation of the moduli and yield strength with distance to the rigidity threshold predicted for ordered packings and measured for disordered emulsions strongly indicates that one has to go beyond models of ordered packings.

2.1.2. Effective medium theory for granular media. For granular media an important question has been to predict the bulk elasticity, and Makse and co-workers have carried out extensive studies of the variation of the elastic moduli and sound propagation speed with pressure in granular media from the perspective of effective medium theory [20–22].

Effective medium theory (EMT) basically assumes that: (i) macroscopic, averaged quantities can be obtained by a simple coarse graining procedure over the individual contacts and (ii) the effect of global forcing, e.g. imposing a deformation, trivially translates to changes in the local contacts. This second assumption is the 'affine assumption' and this will be the crucial assumption that breaks down near jamming.

Makse *et al* studied the breakdown of effective medium theory in the context of granular media. Assuming a Hertzian interaction between spherical grains [23], the contact force f scales with the overlap δ between particles as $f \sim \delta^{3/2}$. As a result, the stiffness of these contacts then scales as $\partial_\delta f \sim \delta^{1/2}$. Since, to a good approximation, the pressure $P \sim f$, one obtains that the stiffness of the individual contacts scales as $P^{1/3}$. EMT then predicts that the elastic bulk modulus K and shear modulus G scale as the stiffness of the contacts: $K \sim G \sim P^{1/3}$, and that the sound velocities scale as $P^{1/6}$ [20–22, 24]. In particular, the ratio G/K should be independent of pressure.

From a range of simulations Makse *et al* concluded that the affine assumption works well for the compression modulus, provided that the change in contact number with P is taken into account, but fails for the shear modulus and they suggested that this is due to the non-affine nature of the deformations [20–22]. We will discuss this issue at length in section 3.

2.2. Beyond affine approaches

In a seminal paper in 1990, Bolton and Weaire asked how a *disordered* foam loses rigidity when its gas fraction is decreased [15]. They probed this question by simulations of a two-dimensional polydisperse foam, consisting of approximately a hundred bubbles, as a function of ϕ (figure 2). Their model captures the essential surface-tension-driven structure of foams and predates the now widely used 'surface evolver' code for foams [26].

The following crucial observations are made: (i) the critical density is around 0.84, which is identified as the random close packing density in two dimensions—here the yield stress appears to vanish smoothly. (ii) The contact number z smoothly decreases with ϕ. At $\phi = 1$ the contact number equals 6. This can be understood by combining Euler's theorem which relates the number of vertices, faces and edges in tilings with Plateau's rule that, for a two-dimensional dry foam in equilibrium, three films (faces) meet in one point (vertex). When $\phi \to \phi_c$, the contact number appears to reach the marginal value of 4. (iii) The shear modulus decreases with ϕ and appears to smoothly go to zero at $\phi = \phi_c$ (unfortunately the authors do not comment on the bulk modulus).

In related work on the so-called bubble model developed for wet foams in 1995, Durian reached similar conclusions for two-dimensional model foams and moreover found that the contact number indeed approaches $4(=2d)$ near jamming and observed the non-trivial square root scaling of $z - 4$ with excess density for the first time (figure 3). All these findings are consistent with what is found in closely related models of frictionless soft spheres near jamming, as discussed in section 3.

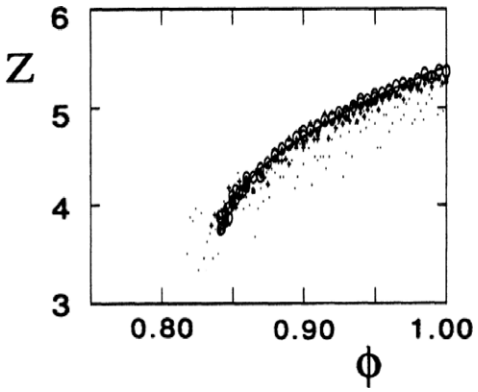

Figure 3. Square root scaling of contact number z with $\phi - \phi_c$ observed in the Durian bubble model (adapted from [25] with permission—copyright by the American Physical Society).

Experimentally, measurements of the shear modulus and osmotic pressure of compressed three-dimensional monodisperse but disordered emulsions found similar behavior for the loss of rigidity [27–29]. The shear modulus (when scaled appropriately with the Laplace pressure, which sets the local 'stiffness' of the droplets) grows continuously with ϕ and vanishes at $\phi_c \approx 0.635$, corresponding to random close packing in three dimensions. The osmotic pressure exhibits very similar scaling, implying that the bulk modulus (being proportional to the derivative of the pressure with respect to ϕ) scales differently from the shear modulus—the difference between shear and bulk modulus is another hallmark of the jamming of frictionless spheres.

There is thus a wealth of simulational and experimental evidence that invalidates simple predictions for the rigidity of disordered media based on our intuition for ordered packings. The crucial ingredient that is missing is the non-affine nature of the deformations of disordered packings (figure 4). There is no simple way to estimate the particle's motion and deformations in disordered systems, and one needs to resort to (numerical) experiments. Jamming can be seen as the avenue that connects the results of such experiments. Jamming aims at capturing the mechanical and geometric properties of disordered systems, building on two insights: first, that the non-affine character becomes large near the jamming transition, and second, that disorder and non-affinity are not weak perturbations away from the ordered, affine case, but may lead to completely new physics [24, 27, 32–36].

3. Jamming of soft frictionless spheres

Over the last decade, tremendous progress has been made in our understanding of what might be considered the 'Ising model' for jamming: static packings of soft, frictionless

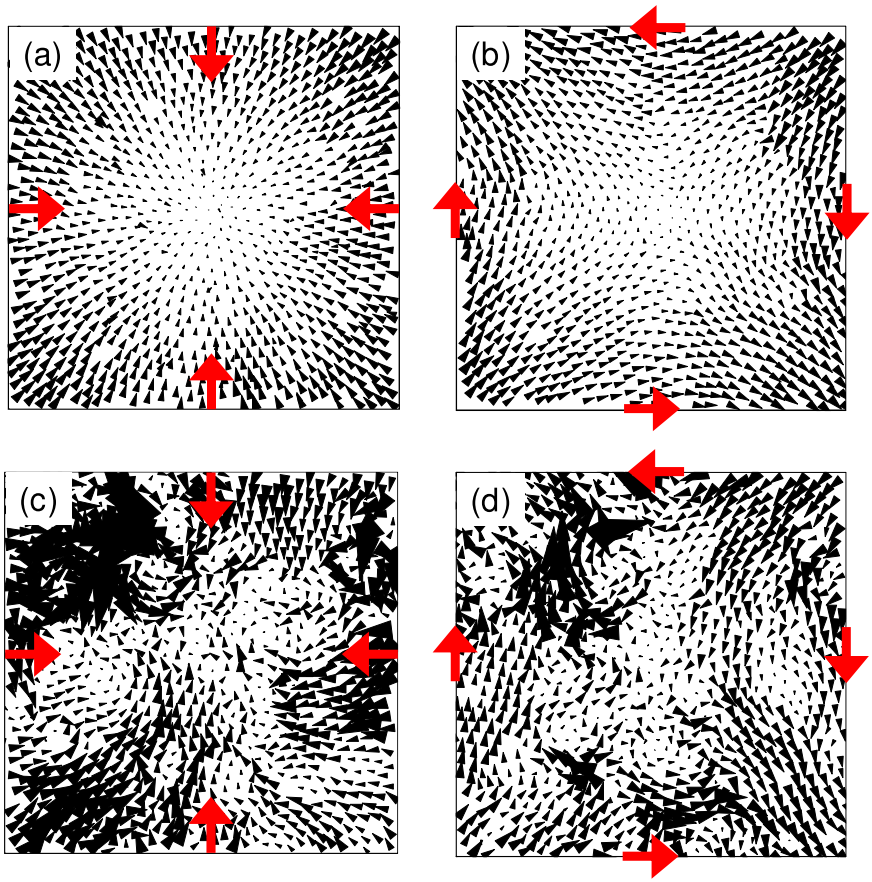

Figure 4. Deformation fields of packings of 1000 frictionless particles under compression ((a), (c)) and shear ((b), (d)) as indicated by the red arrows. The packings in the top row ((a), (b)) are strongly jammed (contact number $z = 5.87$), while the packings in the bottom row ((c), (d)) are close to the jamming point—their contact number is 4.09, while the jamming transition occurs for $z = 4$ in this case. Clearly, the deformation field becomes increasingly non-affine when the jamming point is approached (adapted from [30, 31] with permission—copyright by the American Physical Society).

spheres that act through purely repulsive contact forces. In this model, temperature, gravity and shear are set to zero. The beauty of such systems is that they allow for a precise study of a jamming transition. As we will see in sections 4 and 5, caution should be applied when applying the results for soft frictionless spheres to frictional and/or non-spherical particles.

From a theoretical point of view, packings of soft frictionless spheres are ideal for three reasons. First, they exhibit a well-defined jamming point: for positive P the system is jammed, as it exhibits a finite shear modulus and a finite yield stress [2], while at zero pressure the system loses rigidity. Hence, the (un)jamming transition occurs when the pressure P approaches zero, or, geometrically, when the deformations of the particles vanish. The zero-pressure, zero-shear, zero-temperature point in the jamming phase diagram is referred to as 'point J' (figures 1(e) and 5). In this review, point J will only refer to soft frictionless spheres and not to jamming transitions of other types of particles. Second, at point J the contact number approaches the so-called isostatic value and the system is marginally stable. The system's mechanical and geometrical properties are rich and peculiar here. For large systems the critical packing density, ϕ_c, approaches values usually associated with random close packing. Third, the mechanical and geometrical properties of jammed systems at finite pressure, or equivalently $\phi - \phi_c > 0$, exhibit non-trivial power law scalings as a function $\Delta\phi := \phi - \phi_c$ or, similarly, as a function of the pressure, P.

In this section we address the special nature of point J and discuss the scaling of the mechanical and geometrical properties for jammed systems near point J. We start in section 3.1 with a brief discussion of a few common contact laws and various numerical protocols used to generate jammed packings. We then present evidence that the jamming transition of frictionless spheres is sharp and discuss the relevant control parameters in section 3.2. In section 3.3 we discuss the special geometrical features of systems at point J, as probed by the contact number and pair correlation function. Away from point J the contact number exhibits non-trivial scaling, which appears to be closely related to the pair correlation function at point J, as discussed in section 3.4. Many features of systems near point J can be probed in linear response, and these are discussed at length in section 3.5—these include the density of states (3.5.1), diverging length and timescales (3.5.2), elastic moduli (3.5.3) and non-affine displacements (3.5.4). We close this section by a comparison of effective medium theory, rigidity percolation and jamming, highlighting the unique nature of jamming near point J (3.5.5).

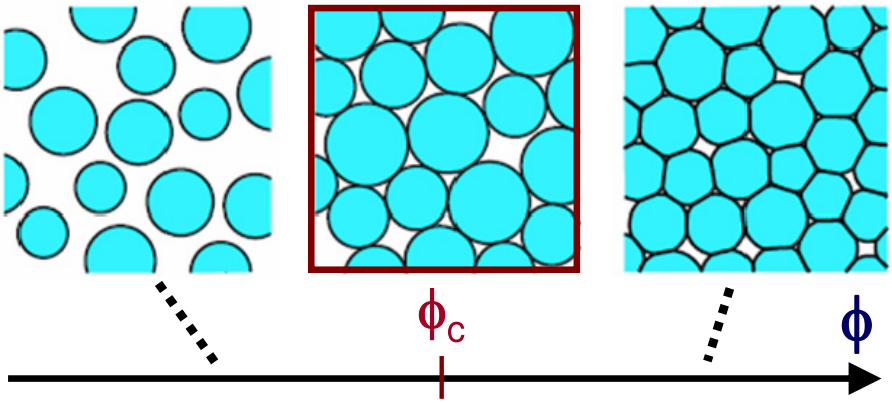

Figure 5. States of soft frictionless spheres as a function of packing density ϕ, below, at and above the critical density ϕ_c. Left: unjammed system at a density below the critical density—pressure is zero and there are no contacts. Middle: marginally rigid system consisting of undeformed frictionless spheres just touching. The system is at the jamming transition (point J), has vanishing pressure, critical density and $2d$ contacts per particle, where d is the dimension. Right: jammed system for finite pressure and density above ϕ_c.

3.1. Definition of the model

At the (un)jamming transition soft particles are undeformed and the distance to jamming depends on the amount of deformation. Rigid particles are therefore always at the jamming transition, and soft particles are necessary to vary the distance to point J. Deformable frictionless spheres interact through purely repulsive body centered forces, which can be written as a function of the amount of virtual overlap between two particles in contact. Denoting the radii of particles in contact as R_i and R_j and the center-to-center distance as r_{ij}, it is convenient to define a dimensionless overlap parameter δ_{ij} as

$$\delta_{ij} := 1 - \frac{r_{ij}}{R_i + R_j}, \tag{1}$$

so that particles are in contact only if $\delta_{ij} \geqslant 0$. We limit ourselves here to interaction potentials of the form

$$V_{ij} = \epsilon_{ij}\delta_{ij}^{\alpha} \qquad \delta_{ij} \geqslant 0, \tag{2}$$

$$V_{ij} = 0 \qquad \delta_{ij} \leqslant 0. \tag{3}$$

By varying the exponent, α, one can probe the nature and robustness of the various scaling laws discussed below. For harmonic interactions, $\alpha = 2$ and ϵ_{ij} sets the spring constant of the contacts. Hertzian interactions between three-dimensional spheres, where contacts are stiffer as they are more compressed, correspond to $\alpha = 5/2$.[1] O'Hern *et al* have also studied the 'Hernian' interaction ($\alpha = 3/2$), which corresponds to contacts that become progressively weaker when compressed [2].

Once the contact laws are given, one can generate packings by various different protocols, of which MD (molecular dynamics) [20–22, 24] and conjugate gradient [2] are the most commonly used[2]. In MD simulations one typically starts simulations with a loose gas of particles, which are incrementally compressed, either by shrinking their container or by inflating their radii. Supplementing the contact laws with dissipation (inelastic collisions, viscous drag with a virtual background fluid, etc) the system 'cools' and eventually one obtains a stationary jammed state. While straightforward, one might worry that statistical properties of packings obtained by such a procedure depend on aspects of the procedure itself—for frictional packings, this is certainly the case [37].

For frictionless particles, the interactions are conservative and one can exploit the fact that stable packings correspond to minima of the elastic energy. Packings can then be created by starting from a completely random configuration and then bringing the system to the nearest minimum of the potential energy. When the energy at this minimum is finite, the packing is at finite pressure, and this procedure is purported to sample the phase space of allowed packings flatly [2, 38]. An effective algorithm to find such minima is known as the 'conjugate gradient technique' [39]. For frictionless systems, we are not aware of significant differences between packings obtained by MD and by this method[3].

Finally it should be noted that, to avoid crystallization, two-dimensional packings are usually made polydisperse, and a popular choice is bidisperse packings where particles of radii 1 and 1.4 are mixed in equal amounts [2, 30]. In three dimensions, this is not necessary as monodisperse spheres then do not appear to order or crystallize for typically employed numerical packing generation techniques.

3.2. Evidence for sharp transition

The seminal work of O'Hern *et al* [2, 40] has laid the groundwork for much of what we understand about jamming of frictionless soft spheres. These authors begin by carefully establishing that frictionless soft spheres exhibit a sharp jamming transition. First, it was found that, when a jammed

[1] When one strictly follows Hertz's law, one finds that ϵ_{ij} depends on the radii R_i and R_j—but often ϵ_{ij} is simply taken as a constant, and for typical polydispersities the effect of this for statistical properties of packings is likely small [31].

[2] For undeformable particles, the Lubachevsky–Stillinger algorithm can be used.

[3] It is an open question whether history never plays a role for frictionless spheres—for example, one may imagine that, by repeated decompression and recompression, different ensembles of packings could be accessed.

packing is decompressed, the pressure, the bulk modulus and the shear modulus vanish at the same critical density ϕ_c. For finite systems, the value of ϕ_c varies from system to system. For systems of 1000 particles the width of the distribution of ϕ_c, W, still corresponds to 0.4% and must therefore not be ignored. Second, it was shown that the width, W, vanishes with the number of particles N as $W \sim N^{-1/2}$—independent of dimension, interaction potential or polydispersity. In addition, the location of the peak of the distribution of ϕ_c, ϕ_0, also scales with N: $\phi_0 - \phi^* = (0.12 \pm 0.03)N^{-1/\nu d}$. Here d is the dimensionality, $\nu = 0.71 \pm 0.08$ and ϕ^* approaches 0.639 ± 0.001 for three-dimensional monodisperse systems.

These various scaling laws suggest that for frictionless spheres the jamming transition is sharp in the limit of large systems. This jamming point is referred to as point J (see figures 1(e) and 5). At the jamming point, the packings consist of perfectly spherical (i.e. undeformed) spheres which just touch (figure 5). The packing fraction for large systems, ϕ^*, reaches values which have been associated with random close packing (RCP) [2, 15]—(∼0.84 in two dimensions, ∼0.64 in three dimensions). It should be noted that the RCP concept itself is controversial [41].

Control parameters. As we will see, the properties of packings of soft slippery balls are controlled by their distance to point J. What is a good control parameter for jamming at point J? The spread in critical density for finite systems indicates that one should not use the density, but only the excess density $\Delta\phi := \phi - \phi_c$ as a control parameter. In other words, fixing the volume is not the same as fixing the pressure for finite systems.

The disadvantage of using the excess density is that it requires deflating packings to first obtain ϕ_c [2]. This extra step is not necessary when P is used as a control parameter, since the jamming point corresponds to $P = 0$—no matter what the system size or ϕ_c is of a given system. While we believe it is much simpler to deal with fixed pressure than with fixed volume, a disadvantage of P is that its relation to $\Delta\phi$ is interaction-dependent: the use of the excess density stresses the geometric nature of the jamming transition at point J.

We suggest that the average overlap $\langle\delta\rangle$ is the simplest control parameter—even though its use is not common. First, $\langle\delta\rangle$ is geometric and interaction-independent and reaches zero at jamming, also for finite systems. Moreover, for finite systems $\langle\delta\rangle$ still controls the pressure and will be very close to $\Delta\phi$. Of course, in infinite systems, control parameters like the pressure P, the average particle overlap $\langle\delta\rangle$ and the density ϕ are directly linked—for interactions of the form equation (2), $P \sim \delta^{\alpha-1} \sim (\Delta\phi)^{\alpha-1}$. Below, we will use a combination of all these control parameters, reflecting the different choices currently made in the field.

3.3. Geometry at point J

At point J, the system's packing geometry is highly non-trivial. First, systems at point J are isostatic [43]: the average number of contacts per particle is sharply defined and equals the minimum required for stability [2, 44, 45]. Second, near jamming $g(r)$ diverges when $r \downarrow 1$ (for particles of radius 1) [42, 46, 47].

Isostaticity. The fact that the contact number at point J attains a sharply defined value has been argued to follow directly from counting the degrees of freedom and constraints [44, 45]. We discuss such counting arguments in detail in the appendix, but give here the gist of the argument for frictionless spheres.

Suppose we have a packing of N soft spheres in d dimensions, and that the contact number, the average number of contacts at a particle, equals z—the total number of contacts equals $zN/2$, since each contact is shared by two particles. First, the resulting packing should not have any floppy modes, deformation modes that cost zero energy in lowest order. As we discuss in the appendix, this is equivalent to requiring that the $Nz/2$ contact forces balance on all grains, which yields dN constraints on $Nz/2$ force degrees of freedom: hence $z \geqslant 2d$. The minimum value of z required is referred to as the isostatic value z_{iso}: for frictionless spheres, $z_{iso} = 2d$.

Second, at point J, since the particles are undeformed, the distance between contacting particles has to be precisely equal to the sum of their radii. This yields $Nz/2$ constraints for the dN positional degrees of freedom: therefore, one only expects generic solutions at jamming when $z \leqslant 2d$.

Combining these two inequalities then yields that the contact number z_c at the jamming point for soft frictionless discs generically will attain the isostatic value: $z_c = z_{iso} = 2d$ [2, 44, 45]. As we will see below, such counting arguments should be regarded with caution, since they do not provide a correct estimate for the contact number at jamming of frictionless ellipsoidal particles [48–50].

Numerically, it is far from trivial to obtain convincing evidence for the approach of the contact number to the isostatic value. Apart from corrections due to finite system sizes and finite pressures, a subtle issue is how to deal with rattlers, particles that do not have any contacts with substantial forces but still arise in a typical simulation. These particles have low coordination number and their overlap with other particles is set by the numerical precision—these particles do not contribute to rigidity. For low pressures, they can easily make up 5% of the particles. An accurate estimate of the contact number then requires one to ignore these particles and the corresponding 'numerical' contacts [2, 70].

Pair correlation function. In simulations of monodisperse spheres in three dimensions, it was found that near jamming $g(r)$ diverges when $r \downarrow 1$ (for particles of radius 1):

$$g(r) \sim \frac{1}{\sqrt{r-1}}. \tag{4}$$

This expresses that at jamming a singularly large number of particles are on the verge of making contact (figure 6) [42, 46]. This divergence has also been seen in pure hard sphere packings [47]. In addition to this divergence, $g(r)$ exhibits a delta peak at $r = 1$ corresponding to the $dN/2$ contacting pairs of particles.

In simulations of two-dimensional bidisperse systems, a similar divergence can be observed, provided one studies $g(\xi)$, where the rescaled interparticle distance ξ is defined as $r/(R_i + R_j)$, and where R_i and R_j are the radii of the undeformed particles in contact [51].

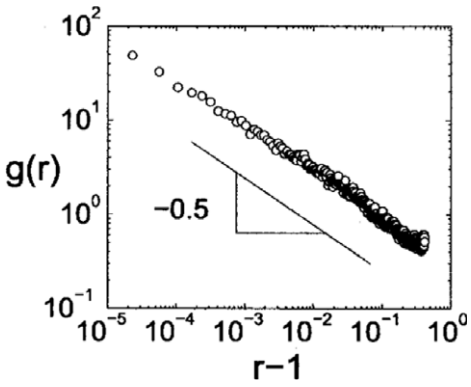

Figure 6. The pair correlation function $g(r > 1)$ of a three-dimensional system of monodisperse spheres of radius 1 illustrates the abundance of near contacts close to jamming ($\Delta\phi = 10^{-8}$ here). Reproduced from [42] with permission—copyright by the American Physical Society.

3.4. Relating contact numbers and packing densities away from J

Below jamming, there are no load bearing contacts and the contact number is zero, while at point J the contact number attains the value $2d$. How does the contact number grow for systems at finite pressure? Assuming that (i) compression of packings near point J leads to essentially affine deformations and that (ii) $g(r)$ is regular for $r > 1$, z would be expected to grow linearly with ϕ: compression by 1% would then bring particles that are separated by less than 1% of their diameter into contact, etc. But we have seen above that $g(r)$ is not regular, and we will show below that deformations are very far from affine near jamming—so how does z grow with ϕ?

Many authors have found that the contact number grows with the square root of the excess density $\Delta\phi := \phi - \phi_c$ [2, 15, 20, 25] (see figure 7). O'Hern *et al* have studied this scaling in detail and find that the excess contact number $\Delta z := z - z_c$ scales as $\Delta z \sim (\Delta\phi)^{0.50\pm0.03}$, where z_c, the critical contact number, is within error bars equal to the isostatic value $2d$ [2]. Note that this result is independent of dimension, interaction potential or polydispersity (see figure 7(a)). Hence, the crucial scaling law is

$$\Delta z = z_0\sqrt{\Delta\phi}, \tag{5}$$

where the precise value of the prefactor z_0 depends on dimension, and possibly weakly on the degree of polydispersity, and is similar to 3.5 ± 0.3 in two dimensions and 7.9 ± 0.5 in three dimensions [2].

The variation of the contact number near J can therefore be perceived to be of mixed first-/second-order character: below jamming $z = 0$, at J the contact number z jumps discontinuously from zero to $2d$, and for jammed systems the contact number exhibits non-trivial power law scaling as a function of increasing density (figures 3 and 7).

We will see below that many other scaling relations (for elastic moduli, for the density of state and for characteristic scales) are intimately related to the scaling of z and the contact number scaling can be seen as the central non-trivial scaling in this system. (In frictional and non-spherical packings, similar scalings for z are found.)

A subtle point is that the clean scaling laws for Δz versus $\Delta\phi$ are only obtained if one excludes the rattlers when counting contacts, but includes them for the packing fraction [2]. Moreover, for individual packings the scatter in contact numbers at a given pressure is quite substantial—see, for example, figure 9 from [52]—and smooth curves such as shown in figure 7(a) can only be obtained by averaging over many packings. Finally, the density ϕ is usually defined by dividing the volume of the undeformed particles by the box size, and packing fractions larger than 1 are perfectly reasonable. Hence, in comparison to packing fractions defined by dividing the volume of the *deformed* particles by the box size, ϕ is larger because the overlap is essentially counted double. Even though none of these subtleties should play a role for the asymptotic scaling close to jamming in large enough systems, they are crucial when compared to experiments and also for numerical simulations.

3.4.1. Connections between contact number scaling, $g(r)$ and marginal stability. The scaling of Δz can be related to the

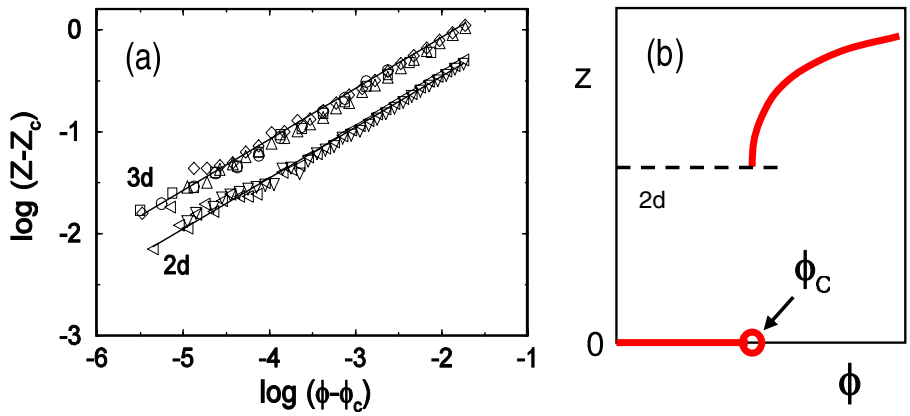

Figure 7. (a) Excess contact number $z - z_c$ as a function of excess density $\phi - \phi_c$. Upper curves represent monodisperse and bidisperse packings of 512 soft spheres in three dimensions with various interaction potentials, while lower curves correspond to bidisperse packings of 1024 soft discs in two dimensions. The straight lines have slope 0.5. Reproduced from [2] with permission—copyright by the American Physical Society. (b) Schematic contact number as a function of density, illustrating the mixed nature of the jamming transition for frictionless soft spheres.

divergence of the radial distribution function as follows [56]. Imagine compressing the packing, starting from the critical state at point J, and increasing the typical particle overlap from zero to δ. If one assumes that this compression is essentially affine, then it is reasonable to expect that such compression closes all gaps between particles that are smaller than δ. Hence

$$\Delta z \sim \int_1^{1+\delta} \mathrm{d}\xi \frac{1}{\sqrt{\xi - 1}} \sim \sqrt{\delta}. \tag{6}$$

Wyart approaches the square root scaling of Δz from a different angle, by first showing that the scaling $\Delta z \sim \sqrt{\delta}$ is consistent with the system staying marginally stable at all densities, and then arguing that the divergence in $g(r)$ is a necessary consequence of that [54]. Both his arguments require assumptions which are not self-evident, though [52].

3.5. Linear response and dynamical matrix

A major consequence of isostaticity at point J is that packings of soft frictionless spheres exhibit increasingly anomalous behavior as the jamming transition is approached. That anomalies occur near jamming is ultimately a consequence of the fact that the mechanical response of an isostatic system cannot be described by elasticity—isostatic systems are essentially different from ordinary elastic systems [45, 55].

In principle these anomalies can be studied at the jamming point: however, much insight can be gained by exploring the mechanical properties as a function of distance to the isostatic point. Below we review a number of such non-trivial behaviors and scaling laws that arise near point J. We will focus on the response to weak quasistatic perturbations, and on the vibrational eigenfrequencies and eigenmodes of weakly jammed systems. Both are governed by the dynamical matrix of the jammed packing under consideration.

For linear deformations, the changes in elastic energy can be expressed in the relative displacement $\mathbf{u}_{ij}$ of neighboring particles i and j. It is convenient to decompose $\mathbf{u}_{ij}$ into components parallel ($u_\parallel$) and perpendicular ($u_\perp$) to $\mathbf{r}_{ij}$, where $\mathbf{r}_{ij}$ connects the centers of particles i and j (figure 8). In these terms the change in energy takes a simple form [31, 43, 54]:

$$\Delta E = \frac{1}{2} \sum_{i,j} k_{ij} \left(u_{\parallel,ij}^2 - \frac{f_{ij}}{k_{ij} r_{ij}} u_{\perp,ij}^2 \right), \tag{7}$$

where f_{ij} and k_{ij} denote the contact forces and stiffnesses. For power law interactions of the form given in equation (2), we can rewrite this as [30]

$$\Delta E = \frac{1}{2} \sum_{i,j} k_{ij} \left(u_{\parallel,ij}^2 - \frac{\delta_{ij}}{\alpha - 1} u_{\perp,ij}^2 \right). \tag{8}$$

The dynamical matrix $\mathcal{M}_{ij,\alpha\beta}$ is obtained by rewriting equation (7) in terms of the independent variables, $u_{i,n}$, as

$$\Delta E = \tfrac{1}{2} \mathcal{M}_{ij,nm} u_{i,n} u_{j,m}. \tag{9}$$

Here $\mathcal{M}$ is a $\mathrm{d}N \times \mathrm{d}N$ matrix with N the number of particles, indices n, m label the coordinate axes and the summation convention is used.

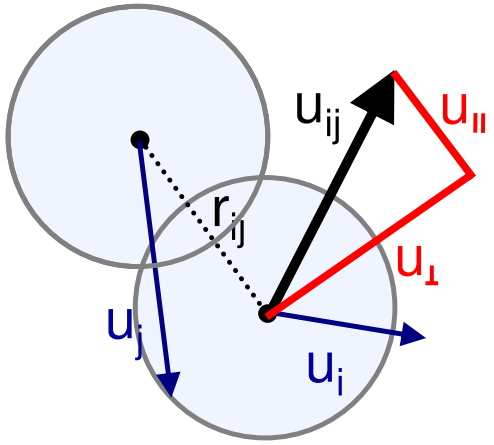

Figure 8. Definition of relative displacement u_{ij}, $u_\parallel$ and $u_\perp$.

The dynamical matrix contains all information on the elastic properties of the system. By diagonalizing the dynamical matrix one can probe the vibrational properties of systems near jamming [2, 33, 54, 56] (see section 3.5.1). The dynamical matrix also governs the elastic response of the system to external forces f^{ext} (see sections 3.5.2–3.5.4) [30, 57]:

$$\mathcal{M}_{ij,nm} u_{j,m} = f_{i,n}^{\mathrm{ext}}. \tag{10}$$

3.5.1. Density of states. Studies of the vibrational modes and the associated density of (vibrational) states (DOS) have played a key role in identifying anomalous behavior near point J. Low frequency vibrations in ordinary crystalline or amorphous matter are long-wavelength plane waves. Counting the number of these, one finds that the density of vibrational states $D(\omega)$ is expected to scale as $D(\omega) \sim \omega^{d-1}$ for low frequencies—this is called Debye behavior. Jammed packings of frictionless spheres do show Debye-like behavior far away from jamming, but as point J is approached, both the structure of the modes and the density of states exhibit surprising features [2, 54, 56, 58].

The most striking features of the density of states are illustrated in figure 9. First, far above jamming, the DOS for small frequencies is regular (black curve). Second, approaching point J, the density of vibrational state DOS at low frequencies is strongly enhanced. (In analogy to what is observed in glasses, this is sometimes referred to as the boson peak, since the ratio of the observed DOS and the Debye prediction exhibits a peak at low ω.) More precisely, the DOS becomes essentially constant up to some low frequency crossover scale at $\omega = \omega^*$, below which the continuum scaling $\sim w^{d-1}$ is recovered. Third, the characteristic frequency ω^* vanishes at point J as $\omega^* \sim \Delta z$.

The density of states thus convincingly shows that, close to the isostatic point/jamming point, the material is anomalous in that it exhibits an excess of low frequency modes, and that at point J the material does not appear to exhibit any ordinary Debye/continuum behavior as here the DOS becomes flat. Jamming of frictionless spheres thus describes truly new physics.

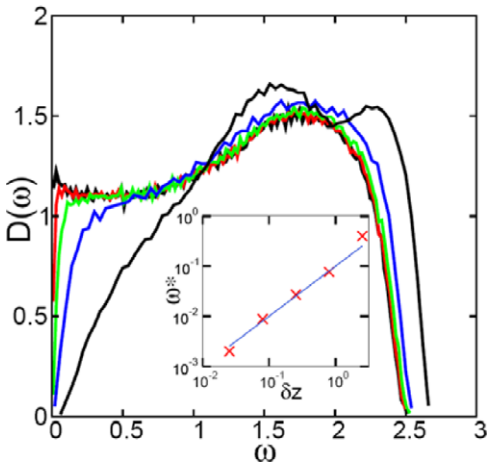

Figure 9. Density of vibrational states $D(\omega)$ for 1024 spheres interacting with repulsive harmonic potentials. Distance to jamming $\Delta\phi$ equals 0.1 (black), 10^{-2} (blue), 10^{-3} (green), 10^{-4} (red) and 10^{-8} (black). The inset shows that the characteristic frequency ω^*, defined as where $D(\omega)$ is half of the plateau value, scales linearly with Δz. The line has slope 1. Adapted from [54, 56] with permission—copyright by the Institute of Physics.

Normal modes. The nature of the vibrational modes changes strongly with frequency and, to a lesser extent, with distance to point J. Various order parameters can be used to characterize these modes, such as the (inverse) participation ratio, level repulsion and localization length [58, 59]. The participation ratio for a given mode is defined as $\mathcal{P} = (1/N)\ (\Sigma_i |u_i|^2)^2 / \Sigma_i |u_i|^4$, where u_i is the polarization vector of particle i [58]. It characterizes how evenly the particles participate in a certain vibrational mode—extended modes have $\mathcal{P}$ of order one, while localized modes have smaller $\mathcal{P}$, with hypothetical modes where only one particle participates in reaching $\mathcal{P} = 1/N$.

Studies of such order parameters have not found very sharp changes in the nature of the modes either with distance to jamming or with eigenfrequency [58–60]. It appears to be more appropriate to think in terms of typical modes and crossovers. Qualitatively, one can consider the DOS to consist of roughly three bands: a low frequency band where $D(\omega) \sim \omega^{d-1}$, a middle frequency band where $D(\omega)$ is approximately flat, and a high frequency band where $D(\omega)$ decreases with ω [58].

Representative examples of modes in these three bands are shown in figure 10. The modes in the low frequency band come in two flavors: plane-wave-like with $\mathcal{P} \sim 1$ and quasi-localized with small $\mathcal{P}$ [59, 60]. The modes in the large frequency band are essentially localized with small $\mathcal{P}$. The vast majority of the modes are in the mid-frequency band (especially close to jamming) and are extended but not simple plane waves—typically the eigenvectors have a swirly appearance.

The localization length ξ of these modes has been estimated to be large, so that many modes have ξ comparable to or larger than the system size. Consistent with this, the modes in the low and mid-frequency range are mostly extended, $\xi > L$, and exhibit level repulsion (i.e. the level spacing statistics $P(\Delta\omega)$ follows the so-called Wigner surmise of random matrix theory), while the high frequency modes are localized ($\xi < L$) and exhibit Poissonian level statistics [59].

When point J is approached, the main change is that the low frequency, 'Debye' range shrinks, and that both the number of plane waves and of quasi-localized resonances diminishes [58–60].

3.5.2. Characteristic length and timescales. The vanishing of the characteristic frequency ω^* at point J suggests searching for a diverging length scale. Below we give an analytical estimate for this length scale and discuss indirect and direct observations of this length scale in simulations.

Estimate of l^*. As pointed out by Wyart *et al* [54], if we cut a circular blob of radius ℓ from a rigid material, it should remain rigid. The rigidity (given by the shear modulus) of jammed materials is proportional to Δz. The circular blob has of the order of $\ell^d \Delta z$ excess contacts. By cutting it out, one breaks the contacts at the perimeter, of which there are of the order of $z\ell^{d-1}$. If the number of broken contacts at the edge is larger than the number of excess contacts in the bulk, the resulting blob is not rigid but floppy: it can be deformed without energy cost (in lowest order). The smallest blob one can cut out without it being floppy is obtained when these numbers are equal, which implies that it has radius $\ell^* \sim z/\Delta z$. Close to the jamming transition, z is essentially constant and so one obtains as a scaling relation that [54]

$$\ell^* \sim \frac{1}{\Delta z}. \tag{11}$$

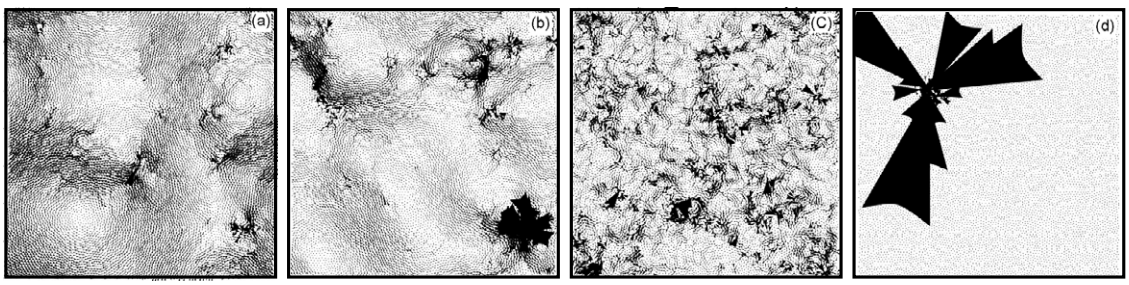

Figure 10. Representative eigenmodes for a two-dimensional system of 10^4 particles interacting with three-dimensional Hertzian interactions ($\alpha = 5/2$, see equation (2)) at a pressure far away from jamming ($z \approx 5.09$). For all modes, the length of the vectors $\propto u_i$ is normalized such that $\sigma_i |u_i|^2$ is a constant. (a) Continuum-like low frequency mode at $\omega \approx 0.030$, $\mathcal{P} \approx 0.79$ and $i_\omega = 3$, where i_ω counts the non-trivial modes, ordered by frequency. (b) Quasi-localized low frequency mode at $\omega \approx 0.040$, $\mathcal{P} \approx 0.06$ and $i_\omega = 7$. (c) Disordered, 'swirly' mid-frequency mode at $\omega \approx 0.39$, $\mathcal{P} \approx 0.31$ and $i_\omega = 1000$. (d) Localized high frequency mode at $\omega \approx 4.00$, $\mathcal{P} \approx 0.0013$ and $i_\omega = 9970$.

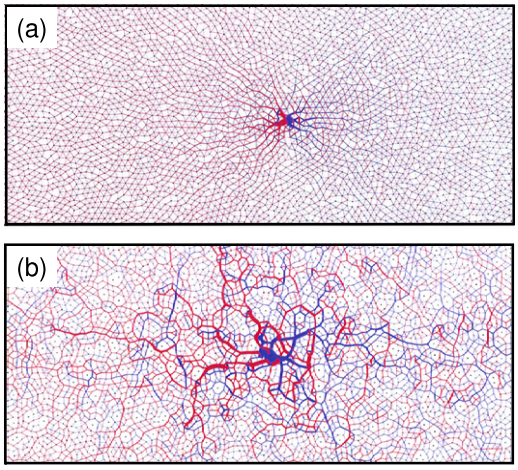

Figure 11. Divergence of a characteristic length scale near jamming as observed in the fluctuations of the changes of contact forces of a system of 10^4 Hertzian discs. Blue (red) bonds correspond to increased (decreased) force in response to pushing a single particle in the center of the packing to the right. In panel (a), the system is far from jamming and $z = 5.55$, while in panel (b), the system is close to jamming and $z = 4.05$ (adapted from [31]).

Observation of l^* in vibration modes. Using the speed of sound one can translate the crossover frequency ω^* into a wavelength, which scales as $\lambda_T \sim 1/\sqrt{\Delta z}$ for transverse (shear) waves and as $\lambda_L \sim 1/\Delta z$ for longitudinal (compressional) waves—the difference in scaling is due to the difference in scaling of shear and bulk moduli (see section 3.5.3 below). By examining the spatial variation of the eigenmode corresponding to the frequency ω^*, λ_T has been observed by Silbert *et al* [56]. Notice, however, that the scaling of λ_T is different from the scaling of l^*—it is λ_L that coincides with the length scale ℓ^* derived above.

Observation of l^* in point response. The signature of the length scale ℓ^* can be observed directly in the point force response networks: close to point J, i.e. for small Δz, the scale up to which the response looks disordered becomes large (see figure 11) [30, 31]. By studying the radial decay of fluctuations in the response to the inflation of a single central particle (which is more symmetric than that of point forcing, as shown in figure 11) as a function of distance to jamming, one obtains a crossover length l^* which, as the theoretically derived length scale, varies as $l^* \approx 6/\Delta z$ [31].

Characteristic length and validity of elasticity. An important issue, which has in particular been studied extensively in the context of granular media, is whether elasticity can describe a system's response to, for example, point forcing [55, 61]. Extensive observations of the linear response, connected to the direct observation of l^*, suggest that there is a simple answer and that the distance to the isostatic limit is crucial [30, 31]: below a length scale l^* the response is dominated by fluctuations, and the deformation field can be seen as a distorted floppy mode, while at larger length scales the system's response crosses over to elasticity. This is for a single realization—it can also be shown that, even close to jamming, the ensemble averaged response of a weakly jammed system is consistent with elasticity, provided the correct values of the elastic moduli are chosen—these moduli are consistent with the globally defined ones [31].

3.5.3. Scaling of shear and bulk moduli. The scaling of the shear modulus, G, and bulk modulus, K, plays a central role in connecting the non-affine, disordered nature of the response to the anomalous elastic properties of systems near jamming. To understand why disorder is so crucial for the global, mechanical response of a collection of particles that act through short range interactions, consider the local motion of a packing of spherical, soft frictionless spheres under global forcing. The global stresses can be obtained from the relative positions $\vec{r}_{ij}$ and contact forces $\vec{f}_{ij}$ of pairs of contacting particles i and j via the Irving–Kirkwood equation:

$$\Sigma_{\alpha\beta} = \frac{1}{2V}\Sigma_{ij} f_{ij,\alpha} r_{ij,\beta}, \tag{12}$$

where σ_{ab} is the stress tensor, α and β label coordinates and V is the volume.

Once we know the local motion of the particles in response to an externally applied deformation, we can calculate the contact forces from the force law and thus obtain the stress in response to deformation. Let us first estimate the scaling of the moduli from the affine prediction where one assumes that the typical particle overlap δ is proportional to $\Delta\phi$ and that all bonds contribute similarly to the increase in elastic energy when the packing is deformed. For a deformation strain ε we can estimate the corresponding increase in energy from equation (8) as $\Delta E \sim \Sigma k\varepsilon^2$. Therefore, under affine deformations, the corresponding elastic modulus is of order k—in other words, the elastic moduli simply follow from the typical stiffnesses of the contacts.

Consider now deforming a *disordered* jammed packing. All particles feel a local disordered environment and deformations will not be affine (figure 4). The point is that these non-affine motions become increasingly strong near the jamming transition and qualitatively change the scaling behavior of, for example, the shear modulus of foams and granular media [2, 15, 20, 43, 62].

A particularly enlightening manner to illustrate the role of non-affine deformations is to initially force the particle displacements to be affine and then let them relax. In general, the system can lower its elastic energy by additional non-affine motions. Calculating the elastic energies of enforced affine deformations and of the subsequent relaxed packings of soft frictionless spheres, O'Hern *et al* found that the non-affine relaxation lowers both the shear and bulk modulus, but crucially changes the scaling of the shear modulus with distance to jamming [2]—see figure 12.

In general, one finds that, for power law interactions (equation (2)), the pressure scales as $\Delta\phi^{\alpha-1}$ and the contact stiffness k and bulk modulus K scale as $\Delta\phi^{\alpha-2}$ [2, 30, 62]. The surprise is that the shear modulus G gets progressively smaller as the bulk modulus near point J, and G scales differently from K with distance to jamming: $G \sim \Delta\phi^{\alpha-3/2}$ (see figure 12) [2, 20, 30, 62]. The relations between the scaling of G, K and k can be rewritten as

$$G \sim \Delta z K \sim \Delta z k. \tag{13}$$

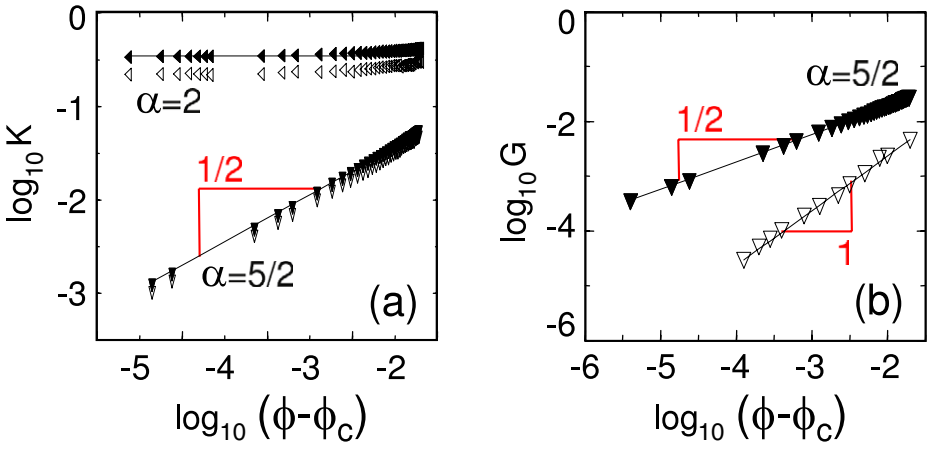

Figure 12. Bulk (K) and shear (G) modulus as a function of distance to jamming for two-dimensional bidisperse systems, with interaction potential $V \sim \delta^\alpha$ (see equation (2)). The closed symbols denote moduli calculated by forcing the particles to move affinely and the open symbols correspond to the moduli calculated after the system has relaxed. Slopes are as indicated (adapted from [2] with permission—copyright by the American Physical Society).

It is worth noting that many soft matter systems (pastes, emulsions) have shear moduli which are much smaller than compressional moduli—from an application point of view, this is a crucial property.

Putting all this together, we conclude that the affine assumption gives the correct prediction for the bulk modulus (since $k \sim \delta^{\alpha-2} \sim \Delta\phi^{\alpha-2}$), but fails for the shear modulus. This failure is due to the strongly non-affine nature of shear deformations: deviations from affine deformations set the elastic constants [2, 20, 30, 43, 62]. As we will see below, the correspondence between the bulk modulus and the affine prediction is fortuitous, since the response becomes singularly non-affine close to point J for both compressive and shear deformations (section 3.5.5).

3.5.4. Non-affine character of deformations. Approaching the jamming transition, the spatial structure of the mechanical response becomes less and less similar to continuum elasticity, but instead increasingly reflects the details of the underlying disordered packing and becomes increasingly non-affine [30]—see figure 4(a). Here we will discuss this in the light of equation (8), which expresses the changes in energy as a function of the local deformations $u_\parallel$ and $u_\perp$: $\Delta E = \frac{1}{2}\sum_{i,j} k_{ij}(u^2_{\parallel,ij} - \frac{\delta_{ij}}{\alpha-1}u^2_{\perp,ij})$.

To capture the degree of non-affinity of the response, Ellenbroek and co-workers have introduced the displacement angle α_{ij}.[4] Here α_{ij} denotes the angle between $\mathbf{u}_{ij}$ and $\mathbf{r}_{ij}$, or

$$\tan\alpha_{ij} = \frac{u_{\perp,ij}}{u_{\parallel,ij}}. \tag{14}$$

The probability distribution $P(\alpha)$ can probe the degree of non-affinity by comparison with the expected $P(\alpha)$ for affine deformations. Affine compression corresponds to a uniform shrinking of the bond vectors, i.e. $u_{\perp,ij} = 0$ while $u_{\parallel,ij} = -\varepsilon r_{ij} < 0$: the corresponding $P(\alpha)$ exhibits a delta peak at $\alpha = \pi$. The effect of an affine shear on a bond vector depends on its orientation, and for isotropic random packings $P(\alpha)$ is flat.

Numerical determination of $P(\alpha)$ shows that systems far away from the jamming point exhibit a $P(\alpha)$ similar to the affine prediction but that, as point J is approached, $P(\alpha)$ becomes increasingly peaked around $\alpha = \pi/2$ (figures 13(b) and (c)). This is reminiscent of the $P(\alpha)$ of floppy deformations, where the bond length does not change and $P(\alpha)$ exhibits a δ peak at $\pi/2$. Hence deformations near jamming become strongly non-affine, and, at least locally, resemble those of floppy modes.

Non-affinity of floppy modes and elastic response. Wyart and co-workers have given variational arguments for deriving bounds on the energies and local deformations of soft (low energy) modes starting from purely floppy (zero energy) modes [54, 63]. They construct trial soft modes that are basically floppy modes, obtained by cutting bonds around a patch of size ℓ^* and then modulating these trial modes with a sine function of wavelength ℓ^* to make the displacements vanish at the locations of the cut bonds [30, 54]. In particular, for the local deformations, they find [63]

$$\frac{u_\parallel}{u_\perp} \sim \frac{1}{\ell^*} \to \frac{u_\parallel}{u_\perp} \sim \Delta z, \tag{15}$$

where symbols without indices ij refer to typical or average values of the respective quantities.

The question is whether the linear response follows this prediction for the soft modes. The width w of the peak in $P(\alpha)$ is, close to the jamming transition, roughly $u_\parallel/u_\perp$ because $|\alpha_{ij} - \pi/2| \approx u_{\parallel,ij}/u_{\perp,ij}$ if $u_{\parallel,ij} \ll u_{\perp,ij}$. It turns out that the scaling behavior (15) is consistent with the width w of the peak of $P(\alpha)$ for shear deformations, but not for compression. There the peak of $P(\alpha)$ does not grow as much and a substantial shoulder for large α remains even close to jamming: the tendency for particles to move towards each other remains much more prominent under compression.

Scaling of $u_\parallel$ and $u_\perp$. The scaling of the distributions of $u_\parallel$ and $u_\perp$ has also been probed. The key observation is that in

[4] Not to be confused by the power law index of the interaction potential.

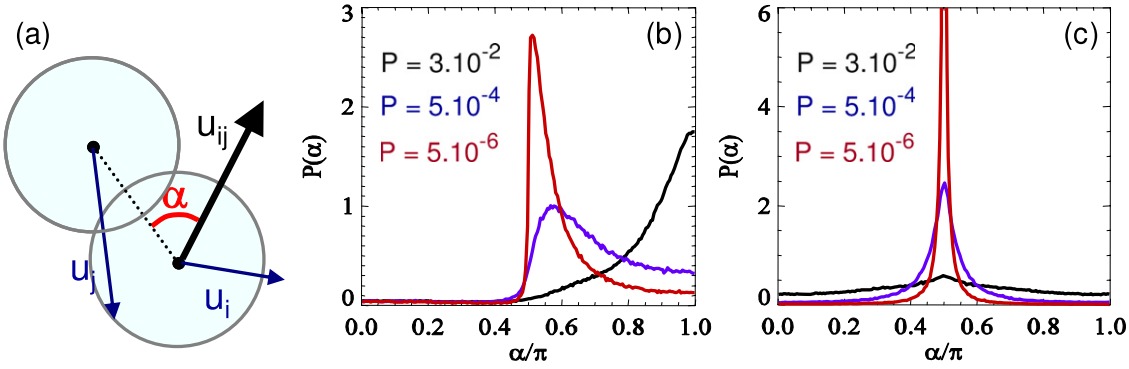

Figure 13. (a) Illustration of definition of displacement angle α. ((b) and (c)) Probability distributions $P(\alpha)$ for compression (b) and shear (c) for Hertzian particles in two dimensions. The three pressures indicated correspond to $z \approx 6.0$, $z \approx 4.5$ and $z \approx 4.1$, respectively (adapted from [30] with permission—copyright by the American Physical Society).

equation (8) the terms $\sim u_\parallel$ and $u_\perp$ have opposite signs. What is the relative contribution of these terms, and can we ignore the latter? Surprisingly, even though $\delta \ll 1$, equation (15) predicts that the two terms are of equal magnitude in soft modes, and so for a linear response one needs to be cautious.

It has become clear that the balance of the terms is never so precise as to qualitatively change the magnitude of the energy changes: ΔE and $\frac{1}{2}\sum_{i,j} k_{ij}(u^2_{\parallel,ij})$ scale similarly [31, 62]. Hence, the typical values of $u_\parallel$ under a deformation are directly connected to the corresponding elastic modulus: for compression $u_\parallel$ is essentially independent of the distance to jamming ($u_\parallel \sim \epsilon$), while for shear $u_\parallel \sim \epsilon\Delta\phi^{1/4}$, where ϵ is the magnitude of the strain [31, 62].

The scaling for $u_\perp$, the amount by which particles in contact slide past each other, is more subtle. Numerically, one observes that, for shear deformations, $u_\perp \sim \epsilon\Delta\phi^{-1/4}$. The two terms $\sim u_\parallel$ and $\sim u_\perp$ become comparable here, and the amount of sideways sliding under a shear deformation diverges near jamming [30, 31, 62]. For compression there is no simple scaling. Combining the observed scaling for $u_\parallel$ with equation (15), one might have expected that $u_\perp \sim \epsilon\Delta\phi^{-1/2}$. However, the data suggests a weaker divergence, close to $\Delta\phi^{-0.3}$. Hence, consistent with the absence of simple scaling of the peak of $P(\alpha)$ for compression, the two terms $\propto u_\parallel$ and $\propto u_\perp$ do not balance for compression. Nevertheless, both under shear and compression, the sliding, sideways motion of contacting particles dominates and diverges near jamming.

3.5.5. Effective medium theory, rigidity percolation, random networks and jammed systems. In 1984, Feng and Sen showed that elastic percolation is not equivalent to scalar percolation, but forms a new universality class [64]. In the simplest realization of rigidity percolation, bonds of a ordered spring network are randomly removed and the elastic response is probed. For such systems, both bulk and shear modulus go to zero at the elastic percolation threshold[5] and at this threshold the contact number reaches the isostatic value $2d$ [65]. Later it was shown that rigidity percolation is singular on ordered lattices [66], but similar results are expected to hold on irregular lattices.

While it has been suggested that jamming of frictionless spheres corresponds to the onset of rigidity percolation [59], there are significant differences, for example that the contact number varies smoothly through the rigidity percolation threshold but jumps at the jamming transition [2]. Nevertheless, it is instructive to compare the response of random spring networks of a given contact number to those of jammed packings—note that the linear response of jammed packings of particles with one-sided harmonic interactions is exactly equivalent to that of networks of appropriately loaded harmonic springs, with the nodes of the network given by the particle centers and the geometry and forces of the spring network determined by the force network of the packing.

In figure 14, a schematic comparison of the variation of the elastic moduli with contact number in effective medium theory, for jammed packings and for random networks, is shown. This illustrates that EMT predicts that the elastic moduli vary smoothly through the isostatic point and that the moduli are of the order of the local spring constant k. This is because effective medium theory is essentially 'blind' to local packing considerations and isostaticity. Thus, besides failing to capture the vanishing of G near jamming, its prediction for the bulk modulus fails spectacularly as well: it predicts finite rigidity below isostaticity. Clearly random networks also fail to describe jammed systems, as for random networks both shear and bulk modulus vanish when z approaches $z_{\rm iso}$—from the perspective of random networks, it is the bulk modulus of jammed systems that behaves anomalously.

By comparing the displacement angle distributions $P(\alpha)$ of jammed systems and random networks under both shear and compression, Ellenbroek *et al* conclude that two cases can be distinguished [62]. In the 'generic' case, all geometrical characterizations exhibit simple scaling and the elastic moduli scale as Δz—this describes shear and bulk deformations of randomly cut networks, as well as shear deformations of jammed packings. Jammed packings under compression form the 'exceptional' case: the fact that the compression modulus remains of the order of k near jamming is reflected in the fact that various characteristics of the local displacements do *not* exhibit pure scaling.

[5] To translate the data for $c11$ and $c44$ as a function of p shown in figure 1, note that $G = C44$ and $K = c11 - c44$. All go to zero linearly in $p - p_c$.

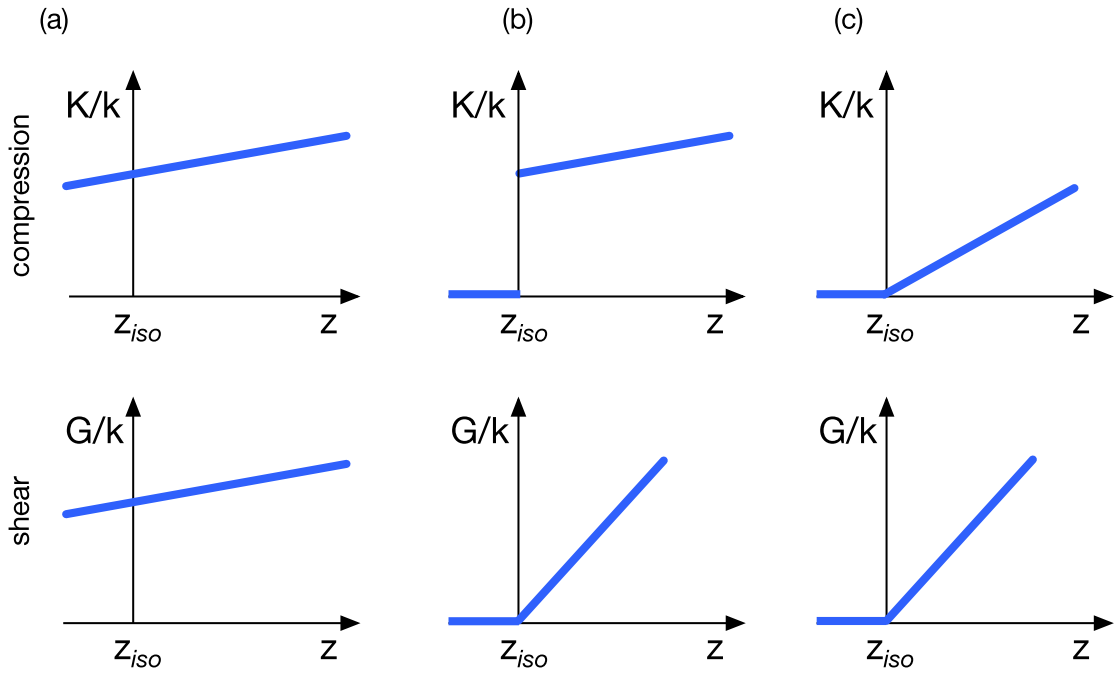

Figure 14. Schematic comparison of the variation of shear (G) and bulk (K) elastic moduli as a function of distance to jamming. (a) In effective medium theory, all elastic moduli are simply of the order of the local spring constant k and, moreover, the theory does not account for whether the packing is rigid or not. (b) In jammed packings of harmonic particles, the bulk modulus K remains constant down to the jamming transition, where it vanishes discontinuously, whereas the shear modulus G vanishes linearly in Δz. (c) In random networks of elastic springs, both elastic moduli vanish linearly with Δz. (Reproduced with permission from [62]—copyright by the Institute of Physics.)

3.6. Conclusion

For packings of soft frictionless spheres and in the limit of large systems, contact number, packing density, particle deformation and (for given a force law) pressure are all directly linked and at point J the system becomes isostatic. The jamming transition for frictionless spheres exhibits a number of non-trivial scaling behaviors, all intimately linked to the non-trivial square root scaling of the excess contact number with distance to the isostatic jamming point. We have stressed the viewpoint that geometry and mechanics are intimately linked for these systems, and that near point J, local non-affinity and global anomalous mechanical scaling go hand in hand.

4. Jamming of frictional spheres

Here we discuss the rich phenomenology of jamming of frictional soft spheres. The crucial difference with the frictionless case is that both the packing density ϕ_c and contact number z_c at jamming are not unique: both depend on the friction coefficient and on the history of the packing, and are lower than for frictionless spheres [37, 46, 67–71]—see figure 15.

Jamming and isostaticity no longer go hand in hand for frictional spheres. The contact number at jamming, z_c, can range from $d + 1$ to $2d$, where $d + 1$ is the isostatic value z_{iso}^{μ} for frictional spheres (see section 4.2.1 and the appendix). It appears that z_c approaches z_{iso}^{μ} only in the limit of $\mu \to \infty$ and very slow equilibration of the packings [69–71]—see section 4.2.4. In all other cases, the number of contacts at jamming is larger than the minimal number needed for force balance and rigidity, and frictional packings of soft spheres at jamming (or, equivalently, frictional rigid spheres) are hyperstatic: $z_c > z_{iso}^{\mu}$. Hyperstaticity implies that, for packings of rigid, frictional spheres, the contact forces are not uniquely determined by the packing geometry, as was the case for the isostatic packings of rigid, frictionless spheres [44, 45]. An explicit example of this so-called indeterminacy of frictional forces is shown in figure 16 [72].

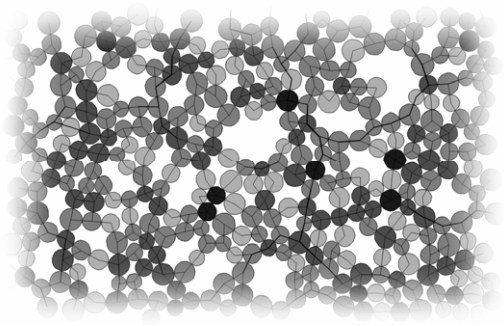

Figure 15. Part of a packing of frictional discs in two dimensions for low pressure, zero gravity and friction coefficient $\mu = 10$. For this packing, $z \approx 3.06$ and $\phi \approx 0.77$ (this density includes rattlers, which are not shown in this image and occur in the 'holes'). Lines indicate the strength of the normal forces—note the large number of near-contacts (pairs of particles appearing to touch but not connected by a force line). Disc color indicates local contact number, clearly identifying the large fraction of particles with two contacts only—these do not arise in frictionless systems.

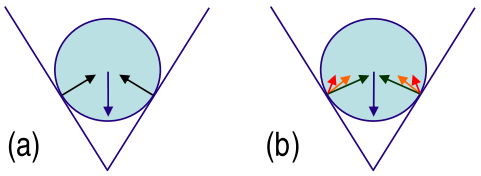

Figure 16. Frictionless (a) and frictional (b) disc in a groove [72]. (a) In the frictionless case, the system is isostatic and the contact forces (black) balancing the gravitational force (blue) are unique. (b) In the frictional case, the system is hyperstatic: contact forces in hard frictional systems are, in general, under-determined. In this example, there are four force degrees of freedom (two normal and two frictional forces) and only three balance equations (total force in x and y directions and torque balance). This leads to a family of solutions (three examples indicated in red, orange and green) that balance the gravitational force (blue). Which of these is realized depends on the history of the system.

What does the deviation of the critical contact number from the isostatic value imply for the scaling of quantities such as G, K and ω^*? We will show that these scale with *distance to the frictional isostatic point*, $z - z_{\rm iso}^{\mu}$. Thus, when the jamming transition is approached, bulk quantities in general do not exhibit scaling with distance to the jamming point since, at jamming, z approaches $z_{\rm c} \geqslant z_{\rm iso}^{\mu}$ [46, 67, 69–71, 73]. Scaling with distance to jamming can only occur when $z_{\rm c} = z_{\rm iso}^{\mu}$. Hence, jamming is not critical for frictional systems: power law scaling of bulk quantities with distance to jamming is the exception, not the rule.

The jamming scenario for frictional soft spheres is detailed below. We briefly discuss the frictional contact laws in section 4.1. In section 4.2 we discuss the properties of frictional sphere packings at the jamming threshold or, equivalently, packings of undeformable frictional spheres. We focus on the variation of the range of contact numbers and densities as a function of μ in sections 4.2.1–4.2.3. Finally in section 4.2.4 we introduce the concept of generalized isostaticity, which is relevant for frictional packings that have fully mobilized contacts. Section 4.3 concerns frictional packings at finite pressures and we discuss the (breakdown) of scaling with distance to jamming.

4.1. Frictional contact laws.

Friction is taken into account by extending the contact force model to account both for normal forces $F_{\rm n}$ and tangential forces $F_{\rm t}$. In the simple Coulomb picture of friction, contacts do not slide as long as the ratio of tangential and normal forces remains smaller than or equal to the friction coefficient μ: $|F_{\rm t}|/F_{\rm n} \leqslant \mu$, which introduces a very sharp nonlinearity in the contact laws. Typical values for μ relevant in experiments range from 0.1 to 1, which is where properties of frictional packs vary strongly with μ.

Frictional forces do not only depend on the relative position of the contacting particles, but also on their history [22, 37, 71–74]. This is encoded in the widely used Hertz–Mindlin model for frictional three-dimensional spheres, which takes the normal force $F_{\rm n} \sim \delta^{3/2}$ with δ the overlap between particles, while the tangential force *increment* $\mathrm{d}F_{\rm t} \sim \delta^{1/2}\,\mathrm{d}t$, where $\mathrm{d}t$ is the relative tangential displacement change, provided $F_{\rm t} \leqslant \mu F_{\rm n}$ [22, 71, 74]. Studies of friction can also be performed for other contact laws, most notably the linear model for which $F_{\rm n} \sim \delta$, so that the stiffness of the contacts in the normal and tangential directions are independent of the normal force and do not vary with distance to jamming [46].

4.2. Frictional packings at zero pressure

4.2.1. Contact number. How can the counting arguments for the contact number at zero pressure be extended to the frictional case? On the one hand, the requirement that contacting spheres precisely touch is the same as for the frictionless case and gives $zN/2$ constraints on the dN particle coordinates, leading to $z \leqslant 2d$. On the other hand, for *frictional* packings, the constraint counting for the $zdN/2$ contact force components constrained by dN force and $d(d-1)N/2$ torque balance equations (see the appendix) gives $z \geqslant d+1$, where the isostatic value $z_{\rm iso}^{\mu} = d+1$. Combining these two bounds, frictional spheres can attain a range of contact numbers: $d+1 \leqslant z_{\rm c} \leqslant 2d$ (see the appendix).

It is important to stress that neither bound is sensitive to the value of μ. What mechanism (if any) selects the contact number $z_{\rm c}$ of a frictional packing at jamming? The first additional ingredient to consider is the Coulomb criterion that for all contact forces $|F_{\rm t}|/F_{\rm n} \leqslant \mu$. So, while constraint counting allows force configurations that satisfy force and torque balance for z arbitrarily close to $z_{\rm iso}^{\mu}$, such configurations are not guaranteed to be compatible with the Coulomb criterion, and in particular for small μ they generally will not be. This is consistent with the intuition that a small increase of μ away from zero is not expected to make $z_{\rm c}$ jump from $2d$ to $d+1$. In section 4.2.4 we will discuss an additional bound on z as a function of μ.

Simulations show that, in practice, $z_{\rm c}$ is a decreasing function of μ, approaching $2d$ at small μ and approaching $d+1$ for large friction coefficient [46, 68–71] (figure 17(a)). However, $z_{\rm c}(\mu)$ cannot be a sharply defined curve unless additional information about the preparation history is given: from the non-sliding condition $|F_{\rm t}|/F_{\rm n} \leqslant \mu$ it follows that a packing which is stable for a certain value of μ remains so for all larger values of μ—increasing the friction coefficient only expands the range of allowed force configurations (and does not change any of the contact forces). Hence, a numerically obtained curve $z_{\rm c}(\mu)$ at best is a bound for the allowed combinations of $z_{\rm c}$ and μ (see figure 17(a)). History is a second additional ingredient to consider [37], although it is remarkable that several different equilibration algorithms appear to give very similar estimates for $z_{\rm c}(\mu)$ [37, 46, 67–71].

4.2.2. Density. The existence of a wide range of statistically different frictional packings is also reflected in packing densities, which experimentally are more easily observed than the contact number. It is well known that packings of spherical hard particles under gravity (in other words, frictional spheres close to jamming) can be compacted over a range of densities [76]. Different packing densities of these systems do not correspond to deformations of the particles, but to changes

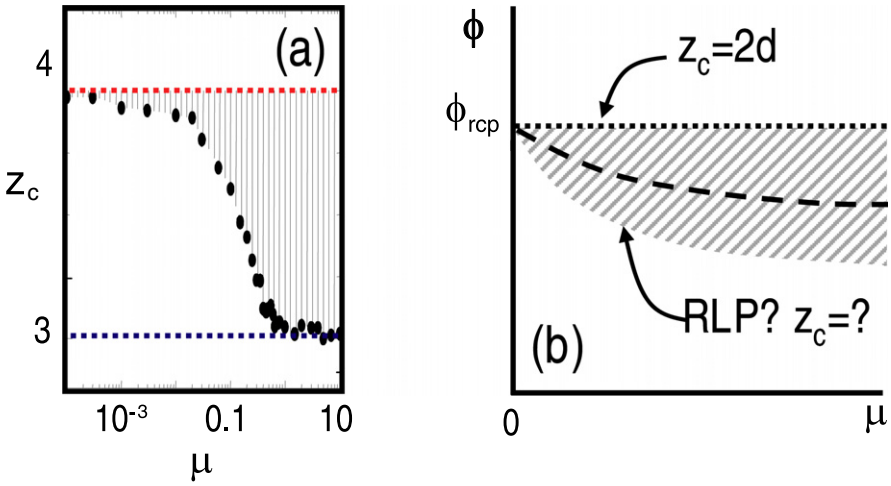

Figure 17. (a) Example of the variation of the zero-pressure contact number z_c in two-dimensional rigid discs as a function of μ, smoothly interpolating between the isostatic limits $2d$ (red) for zero friction and $d+1$ (blue) for frictional contacts. The arched area indicate combinations of contact numbers and μ that, while they are not reached in these numerics, are perfectly possible—see text (adapted from [68]—copyright by the American Physical Society). (b) State diagram for frictional spheres. While the random close packed, isostatic packings obtained for zero friction are compatible with all values of μ, a range of packings with lower densities and contact numbers open up when $\mu > 0$. For a given preparation protocol, there might be a well-defined density (dashed curve). Whether there is a well-defined lowest packing fraction for given μ, which would define random loose packing, is an open question, and the question what the contact number of such states would be is open as well (adapted from [75]).

in the organization of the particles. Hence, at jamming, the range of packing densities does not go to zero for frictional particles.

The relation between density and friction coefficient can be summarized in a simple state diagram (figure 17(b)), which stresses that random close packing (RCP) is independent of μ, while the random loose packing (RLP) density depends strongly on μ, thus connecting random close packing, random loose packing and the value of the friction coefficient [69, 70, 73, 77–80]. This diagram further suggests that the packing density at point J may also be seen as random loose packing of frictionless spheres (since for $\mu = 0$ one expects RCP and RLP to coincide)—it is the loosest possible packings, rather than the densest possible ones, that arise near jamming. It should be noted that the definition of RLP is even more contentious than RCP, and the debate is wide open [73, 78, 79].

4.2.3. Scaling with μ. One may now also wonder how the contact number and packing density at jamming scale with μ. Qualitative evidence for scaling was found by Silbert *et al* in numerical studies of frictional packings (figures 2 and 3 from [46]). By focusing explicitly on a single preparation protocol, such as slow equilibration, this becomes a well-posed question—leading to the concept of generalized isostaticity, defined below. Data for generalized isostatic packings suggests that both contact number and density exhibit power law scaling with μ for small friction, while for large friction, excess contact number and density (defined with respect to the infinite friction limit) are also related by scaling, although clearly more work is needed to establish these scalings firmly [70, 73].

4.2.4. Generalized isostaticity. Here we will discuss the role of the frictional forces in some more detail, and in particular focus on frictional packings for which a large number of contacts are fully mobilized, meaning that the frictional forces are maximal: $|F_t|/F_n = \mu$. These packings arise in numerical studies when packings are equilibrated slowly for a wide range of values of μ.

The mobilization, m, of a contact is defined as the ratio $|F_t|/(\mu F_n)$ and ranges from 0 to 1 (fully mobilized). Earlier numerical data suggested that m generally stays away from 1, and that in the limit of large μ, the distribution of the mobilization $P(m)$ becomes independent of μ [37, 46]. Later it became clear that $P(m)$ can depend strongly on the preparation history [69]. Furthermore, frictional two-dimensional packings which are very slowly equilibrated yield packings for which a substantial amount of the contact forces are fully mobilized, meaning that $|F_t|/F_n = \mu$ [46, 70, 81]. One imagines that, during equilibration, many contacts slowly slide, and when the packing jams many contacts are still close to failure—such packings are marginal with respect to lowering μ.

For packings with fully mobilized contacts, the counting arguments need to be augmented, since at fully mobilized contacts, the frictional and normal forces are no longer independent [70]. Defining the number of fully mobilized contacts per particle as n_m, the constraints for the $zdN/2$ force degrees of freedom then are: dN force balance equations, $d(d-1)N/2$ torque balance equations and $n_m N$ constraints for the fully mobilized contacts. This yields the following relation between z, $z_{iso}^{\mu} = d+1$ and n_m:[6]

$$z - z_{iso}^{\mu} \geqslant 2n_m/d. \tag{16}$$

Surprisingly, for sufficiently slowly equilibrated packings and for all values of μ, the values for n_m and z tend to satisfy this bound when P is lowered to zero (figure 18). Such packings

[6] The corresponding equation in [70] is only correct for $d = 2$.

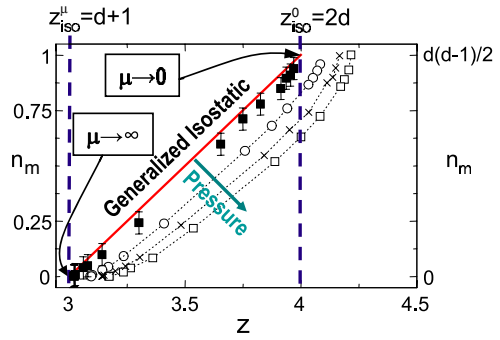

Figure 18. Generalized isostaticity plot, comparing the fraction of fully mobilized contacts per particle, n_m, to the contact number, z. Data points (open symbols) are for two-dimensional systems and for μ ranging from 0.001 to 1000 at finite P. The black squares are the corresponding n_m and z extrapolated to $P = 0$. The left and bottom axes refer to the numerical values for contact number and number of fully mobilized contacts per particle, n_m, for this specific two-dimensional example, while the right and top axes give the corresponding general expressions for higher dimensions. The red line denotes the generalized isostaticity line where the number of fully mobilized contacts is maximized: $n_m = d(z - d - 1)/2$. The area to the right of this line refers to generalized hyperstatic packings, while the area to the left of the red line is forbidden (adapted from [70] with permission—copyright by the American Physical Society).

which maximize their number of fully mobilized contacts have been referred to as 'generalized isostatic' packings [70, 81]. These should be widely occurring, since most preparation algorithms tend to equilibrate slowly [37, 46, 67–71].

For fully mobilized packings, the amount of fully mobilized contacts vanishes in the limit of infinite friction (see figure 18), consistent with the observation that there $z \approx d + 1$. The number of fully mobilized contacts is maximal for vanishingly small friction (which we refer to as $\mu = 0^+$), where, by continuity, $z \approx 2d$ and $n_m \approx d(d-1)/2$. Taking into account that each contact is shared by two particles, the fraction of fully mobilized contacts is $(d-1)/2$—hence in two dimensions 50% of all contacts are fully mobilized, in three dimensions 100% of the contacts would be fully mobilized for $\mu = 0^+$, and in higher dimensions one cannot reach generalized isostaticity for $\mu = 0^+$.

By itself, the inequality (16) is not a stricter bound on z than the ordinary condition $z \geqslant d+1$, since $n_m(\mu)$ is unknown. However, if we could determine $n_m(\mu)$, we would immediately obtain the bound $z = d + 1 + 2n_m(\mu)/d$. It is, at present, an open question how $n_m(\mu)$ can be estimated or obtained numerically other than through direct numerical simulations.

4.3. Frictional packings at finite pressure

Once a mechanically stable frictional packing has been created, its linear mechanical response is given by the dynamical matrix. For Hertz–Mindlin-type interactions, each contact can be thought of as being given by two springs (one parallel to the contact vector r_{ij} and one perpendicular to the contact vector), the spring constants of which are set by the normal force and the Poisson ratio [23].

Various authors have found that, for essentially all values of μ, the excess contact number $z - z_c$ grows as a square root with the excess density [67, 71, 73]—for Hertzian contacts, this is equivalent to stating that $z - z_c \sim P^{1/3}$. However, z_c differs from the frictional isostatic value $d + 1$, so that $z - z^{\mu}_{iso}$ does *not* scale with pressure (see figures 19(a) and (b)). Note that the slope in figure 19(b), which represents the prefactor z_0 in a scaling law of the form $z - z_c = z_0\sqrt{\phi - \phi_c}$, does not appear to vary strongly with μ. As is the case for frictionless particles, it is essential to remove rattlers for the count of the contact number, but include them for the estimate of the density to obtain the square root scaling of $z - z_c$ over an appreciable range [70]. This square root scaling is intriguing and, as far as we are aware, without explanation.

The deviations of z_c from the isostatic value imply that packings near the (un)jamming transition do not approach isostatic packings and, consistent with this, there is, in general, no scaling of the mechanical properties as a function of the distance to jamming.

The mechanical properties do, however, scale with the distance to the isostatic point, as measured by the contact number. First, calculations of the characteristic frequency ω^* from the density of vibrational states for two-dimensional frictional packings show that the variation of ω^* with μ and distance to jamming (as measured by the pressure P) is very similar to that of z (figure 19(c)). In fact, when this data is replotted as a function of $z - z^{\mu}_{iso} = z - 3$ one finds a linear relation between ω^* and $z - z^{\mu}_{iso}$ (figure 19(d)). Second, the ratio of the shear and bulk modulus exhibits the same phenomenology: G/K scales linearly with $z - z^{\mu}_{iso} = z - 3$ (19(e) and (f)) [71, 82]. These findings suggest that, in general, scaling is governed by the distance to isostaticity, rather than the distance to jamming.

The contact number and geometry of the packings change smoothly with μ [71, 73], while the mechanical behavior exhibits a discontinuous jump from $\mu = 0$ to 0^+. This is caused by the fact that, when friction is included, the nature of the dynamical matrix changes completely, because the tangential contact stiffnesses jump from zero to a finite value. When the tangential stiffness is varied smoothly from $\mu = 0$ to finite friction, the mechanical properties vary smoothly also [53].

Finally a word of caution regarding the notion of generalized isostaticity and the role of fully mobilized contacts for scaling away from jamming. In the calculations presented above fully mobilized contacts are treated as ordinary elastic contacts. Strictly speaking, such marginal contacts cause a breakdown of linear response. One may argue that tiny perturbations would simply let the fully mobilized contacts relax to almost-fully-mobilized, after which linear response would no longer be problematic. Taking the opposite view, Henkes *et al* have recently shown that, if the dynamical matrix is calculated under the assumption that fully mobilized contacts can slide freely, the characteristic frequency ω^* scales and vanishes with P for all values of μ—provided one considers systems that approach generalized isostaticity [53].

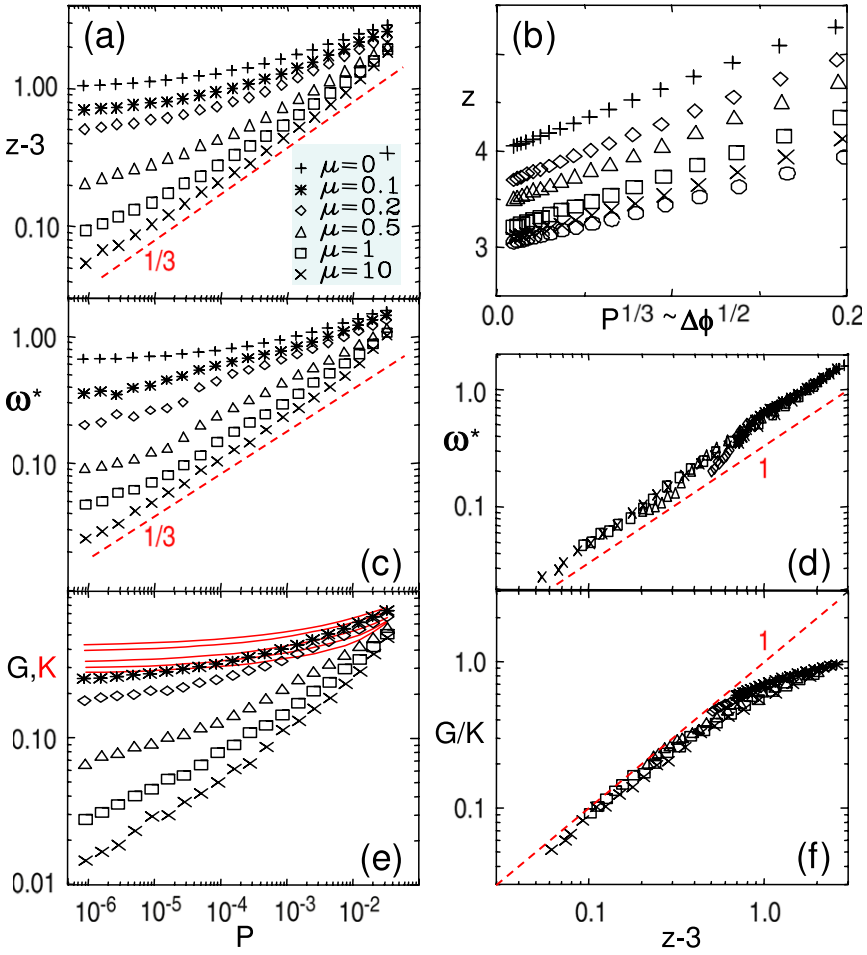

Figure 19. Scaling of contact number, w^* and elastic moduli for frictional discs, interacting through three-dimensional Hertzian–Mindlin forces. (a) The zero-pressure contact number, z_J, does not reach the isostatic limit ($z = 3$) unless μ is very large. (b) The excess coordination number $z - z_J$ scales linearly with $P^{1/3} \sim \sqrt{\Delta\phi}$. ((c) and (d)) The characteristic frequency of the DOS, ω^*, scales similarly to $z - 3$.[7] (e) The bulk modulus K (red curves) approaches a plateau for small P, while G appears to scale as $z - 3$.[8] (f) As in frictionless spheres, the ratio G/K scales with distance to the isostatic point, now given by $z - z^{\mu}_{\rm iso} = z - 3$ (adapted from [71] with permission—copyright by the American Physical Society).

4.4. Conclusion

Jamming of frictional grains can be seen as a two-step process. The first step is the selection of a contact number, z, given the friction coefficient, pressure and procedure. In the second step, in which the mechanical properties of the packing are determined, everything scales with $z - z^{\mu}_{\rm iso}$. The crucial difference with frictionless spheres is that the contact number $z_{\rm c}$ at the $P = 0$ jamming point in general does not coincide with $z^{\mu}_{\rm iso}$. Most quantities are governed by the contact number and scale with distance to isostaticity, while the contact number itself scales with distance to jamming.

5. Jamming of non-spherical particles

New phenomena occur in packings of non-spherical particles, and here we briefly discuss the jamming scenario for frictionless ellipsoids.

First, configurations for hard (or zero-pressure) frictionless ellipsoids pack more densely and have larger contact numbers than frictionless spheres [48–50, 83]. As we discuss in section 5.1, both the increase in density and in contact number away from the sphere limit are continuous but not smooth—plots of ϕ and z as a function of the ellipticity show a cusp at the sphere limit (figure 20).

Second, the counting arguments for general ellipsoids suggest that, at jamming, ellipsoids attain $z = z_{\rm iso} = d(d + 1)$. However, weakly aspherical ellipsoids actually attain a contact number arbitrarily close to the sphere limit $z = 2d$. As a consequence, (weakly) ellipsoidal packings are strongly hypostatic (underconstrained) near jamming. This leads to questions about the relation between contact number, rigidity and floppy modes (section 5.2).

Third, the question arises whether quantities such as z and ω^* exhibit scaling, either as a function of the pressure, as a function of the asphericity or as a function of distance to either the spherical or the ellipsoidal isostatic point—the partial answers to these questions, based on recent studies of the density of states [49, 50], will be addressed in section 5.3.

[7] A trivial scaling of $\omega \sim P^{1/6}$, characteristic for Hertzian contacts, has been scaled out.

[8] A trivial scaling of $K, G \sim P^{1/3}$, characteristic for Hertzian contacts, has been scaled out.

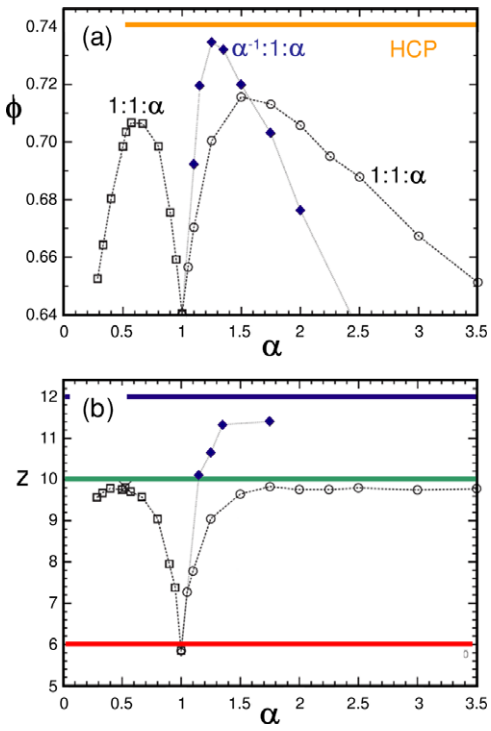

Figure 20. (a) Packing fraction ϕ of spheroids (open symbols) and general ellipsoids (blue symbols) as a function of the asphericity α. The density shows a cusp at $\alpha = 1$ (sphere limit). The orange line indicates the HCP packing density ≈0.74, which is almost reached by random packings of some ellipsoids. (b) The contact number, z, for the same spheroids and ellipsoids as shown in panel (a) also shows a cusp at $\alpha = 1$. The red, green and blue lines at $z = 6$, 10 and 12 indicate the isostatic contact numbers for spheres, spheroids and ellipsoids (adapted from [83]—copyright by The American Association for the Advancement of Science).

5.1. Packings of spherocylinders, spheroids and ellipsoids

Spherocylinders. Early indications for surprisingly dense packings of non-spherical particles come from studies of spherocylinders, particles consisting of a cylinder of length a and diameter 1, which on both ends are capped by a half-sphere. For zero a, these are spheres, while the large a limit is relevant for the loose packings of thin (colloidal) rods [84]. Williams *et al* studied the packing fraction and contact numbers of such spherocylinders numerically and found that both the packing fraction ϕ and contact number z increase when a is increased, reach a maximum for $a \sim 0.4$, and then decrease [85]. The density peaks at a value of 0.695, substantially larger than the typical values for random close packing of spheres ∼0.64, while for large $a > 10$ the density decays as $\phi \sim 1/a$, consistent with arguments given before [84].

The contact number in these simulations was found to start out at $z \approx 5.8$ for $a = 0$ and increased until it reached $z \approx 9$ for $a \approx 0.4$. The initial value is close to the isostatic number for spheres (6), while the peak value is similar to the isostatic number for rods (10) [86][9].

[9] The data also suggested that z decays monotonically for large a but this is likely due to a problem with the contact counting.

Spheroids and ellipsoids. In seminal work, Donev *et al* explored the packing properties of hard spheroids and ellipsoids [83]. As shown in figure 20(a), the density of spheroids (axis: 1:1:α) exhibits a cusp-like local minimum for the pure spherical case $\alpha = 1$ and reaches two local maxima: oblate (disc-like) spheroids at $\alpha \approx 0.6$ pack at a density $\phi \approx 0.70$ and prolate (cigar-shaped) ellipsoids at $\alpha = 1.5$ pack even denser at $\phi \approx 0.715$. Note that the spheroid packing density only drops below the random close packing value for spheres for very strongly oblate ($\alpha \lesssim 0.25$) or prolate ($\alpha \gtrsim 4$) particles.

Even larger packing densities can be obtained for triaxial ellipsoids, and for the case that the axes are given as $1/\alpha$:1:α, the maximum packing density peaks at 0.735 for $\alpha \approx 1.25$ [48, 83]. This density is surprisingly close to the density ≈ 0.74 obtained for fcc and hcp packings, which are the densest possible packings for spheres—but those are crystals, whereas the ellipsoidal packings do not show any appreciable orientational ordering. Finally, crystals of ellipsoids can be packed even denser, with the highest density currently known, 0.7707, is obtained in nonlattice periodic packings of spheroids with either $\alpha \geqslant \sqrt{3}$ or $\alpha \leqslant 1/\sqrt{3}$ [87].

The contact number grows monotonically with asphericity, from a value $\approx 2d$ for the spherical case to values close to the corresponding higher isostatic number for ellipsoids: the contact number for the spheroids measured for strongly oblate or prolate appears to level off at values around 9.8 (the corresponding isostatic number is 10), and for ellipsoids one reaches 11.4 (the corresponding isostatic number is 12) [83]. (The contact numbers in the disordered ellipsoidal systems are difficult to obtain accurately from numerics, in particular for hard particles—since, similar to hard spheres, one expects anomalously many near-contacts [42, 47].) It is noteworthy that the contact numbers reach these asymptotic values at the same asphericities where the density is maximal. Recent work on two-dimensional ellipses [48, 49] and three-dimensional spheroids [50] confirm these trends in contact numbers.

5.2. Counting arguments, floppy modes and rigidity of ellipsoids

The counting arguments for general ellipsoids suggest that, at jamming, ellipsoids attain $z = z_{\rm iso} = d(d+1)$. However, weakly aspherical ellipsoids actually attain a contact number arbitrarily close to the sphere limit $z = 2d$. Hence counting arguments suggest that packings of weakly ellipsoidal particles possess a large number of floppy modes. Are these packings stable?

As a first step in understanding such packings, it is helpful to think about weakly aspherical ellipsoids that approach the sphere limit. The number of floppy modes in such an underconstrained system equals $(N/2)(z_{\rm iso} - z)$, which for the sphere limit (where $z \to 2d$) equals $N(d(d-1)/2)$. What are these floppy modes?

The key observation is that, in the counting arguments for ellipsoids, the rotational degrees of freedom are taken into account while for spheres, where they correspond to trivial rotations of the particles, these are ignored. When these

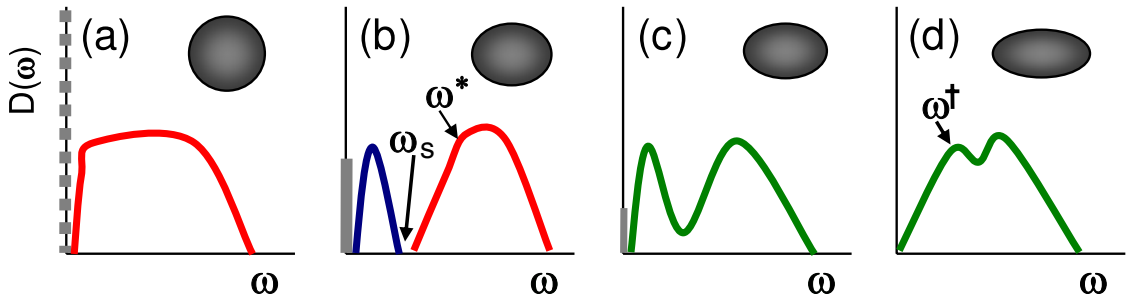

Figure 21. Schematic scenario for the density of states for frictionless soft ellipsoidal particles, based on [49, 50]. ((a)–(d)) Density of states as a function of distance to the spherical limit. The gray, blue, red and green colors refer to floppy modes, rotational modes, translational modes and hybridized modes, respectively. (a) For frictionless spheres, one usually only considers the translational band (red), but when one takes the rotational degrees of freedom into account, a large number of trivial floppy modes occur (dashed gray line). (b) For contact numbers just above $z - z_{\rm iso}^{\rm sphere}$, the density of states exhibits three bands, and the characteristic frequencies $\omega_{\rm s}$ and ω^* scale with asphericity and $z - z_{\rm iso}^{\rm sphere}$, respectively—see text. (c) For contact numbers approaching $z - z_{\rm iso}^{\rm ellip}$, the rotational and translational band merge. (d) For contact numbers above $z - z_{\rm iso}^{\rm ellip}$, there are no floppy modes and the characteristic frequency $\omega^\dagger$ scales with $z - z_{\rm iso}^{\rm ellip}$.

rotational degrees of freedom are also taken into account for frictionless spheres, one obtains precisely $N(d(d-1)/2)$ trivial floppy modes, corresponding to the trivial rotational degrees of freedom of individual frictionless spheres [48, 50]. These floppy modes do not affect the rigidity of the packings, which suggests that, in general, the absence of floppy modes may be a sufficient but not a necessary condition for rigidity [48].

From the perspective of constraint counting of the contact forces, something similar happens in the sphere limit: how do dN force degrees of freedom satisfy both dN force balance equations and also all the additional torque balance equations? The answer is simple: for frictionless spheres, the torques exerted by each contact force are zero, and so torque balance is trivially satisfied.

The key question, however, is what happens to hypostatic packings at *finite* asphericity and pressure. The full answers are not known, but two recent studies on the density of vibrational states for soft frictionless bidisperse two-dimensional ellipses [49] and three-dimensional spheroids [50] provide important ingredients that we will discuss below.

5.3. Jamming of ellipsoids

The main findings for the density of states of ellipsoidal particles are shown in figure 21. Close to the sphere limit, where the contact number is far below the relevant ellipsoidal isostatic value, the density of states consists of three bands: first, a number of zero-frequency, floppy modes corresponding to the degree of hypostaticity, second, a band of rotational modes and third, a band of translational modes, corresponding to the translational modes present for the pure sphere case. When, for increasing pressure and/or strong ellipticity, the contact number starts to approach the ellipsoidal isostatic value, the rotational and translational bands hybridize and merge. Finally, when the contact number exceeds the ellipsoidal isostatic value, the floppy modes have vanished and the characteristic frequency of the remaining single band density of states scales with distance to the ellipsoidal isostatic value.

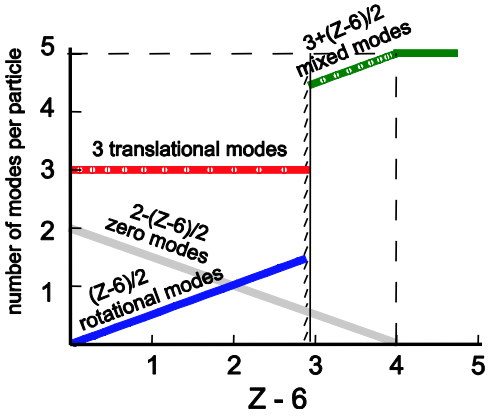

Figure 22. Schematic representation of the number of modes per band for the specific case of spheroids in three dimensions. (Reproduced with permission from [50]—copyright by the Institute of Physics.)

The counting arguments provide a clear picture of the number of modes per band, as shown in figure 22, where the variation of these numbers with contact number is shown for the case of spheroids in 3d.

First, the vibrational modes present for the spherical case are only weakly perturbed by the inclusion of weak ellipticity, so their number still equals dN. The particle motions of modes in this band are essentially translational, and the characteristic frequency of this band, ω^*, still scales with $z - z_{\rm iso}^{\rm sphere}$, *not* with $z - z_{\rm iso}^{\rm ellips}$. Hence, this part of the density of states is smoothly perturbed when going from the sphere to the weakly ellipsoidal case.

Second, for $z < z_{\rm iso}^{\rm ellip}$ the system is underconstrained and the crucial observation is that here there are $(z - z_{\rm iso}^{\rm ellip})/2$ floppy modes. In the sphere limit, these modes are the trivial local rotations, and away from the sphere limit most of these modes survive and become delocalized—their precise nature is not fully understood yet.

Thirds, at finite pressures and/or finite asphericities, $(z - z_{\rm iso}^{\rm sphere})/2$ modes emerge from the zero-frequency band and attain finite frequencies. This is the rotational band: particle

motions of modes in this band are essentially rotational and the vibration frequencies are below those of the translational band. This allows the definition of a characteristic maximal frequency of the rotational band ω_s, which is found to scale with the degree of asphericity $|1 - \alpha|$, but is essentially insensitive to the pressure.

Fourth, for large pressure and asphericity, the contact number approaches the relevant ellipsoidal isostatic number, the rotational and translational bands start to approach each other ($\omega^* - \omega_s \ll 1$), the modes hybridize and these two bands eventually merge. In the regime where the contact number exceeds the relevant ellipsoidal contact number, there are no more floppy modes. The only band of vibrational modes then has a mixed translational/rotational character, and its characteristic frequency, $\omega^\dagger$, scales with distance to the relevant ellipsoidal isostatic point: $\omega^\dagger \sim z - z_{\rm iso}^{\rm ellip}$.

Finally, note that for weakly elliptical systems that are hypostatic, the counting argument implies that the forces must be non-generic—one still has more equations of force and torque balance than one has force degrees of freedom. In terms of the elastic energy landscape, one imagines that near such systems there must exhibit many directions in phase space where the second derivative is zero (leading to quartic modes [49]), but a deep understanding is missing.

5.4. Conclusion

Jamming of frictionless ellipsoidal particles is surprisingly similar to that of frictionless spheres, despite the strongly hypostatic nature of weakly aspherical packings. The crucial observation is that frictionless spheres can also be seen as strongly hypostatic near jamming, as they possess a large number of trivial floppy modes. Most of these modes remain at zero frequency for weakly ellipsoidal particles, even though their spatial structure is no longer trivial, and these modes do not appear to affect the rigidity of packings of frictionless ellipses.

6. Summary, open questions and outlook

The jamming scenario for disordered packings of soft, purely repulsive particles at zero temperature and shear, as described above, can be seen as a two-step process. First, for a given pressure, contact law and preparation protocol, a packing with a certain contact number, z, is created. Second, the mechanical characteristics such as elastic moduli and density of states depend on the difference between the actual contact number and the relevant isostatic value.

Depending on the particles' friction or shape, the contact number may span a range of values—see figure 23 for this range for $P \to 0$. For frictionless particles it appears that the contact number at jamming is independent of the preparation procedure, even for finite pressures. For frictional particles, a range of contact numbers arises and the history becomes crucial.

Jamming of frictionless soft spheres constitutes a special case, since here the isostatic contact number (excluding the trivial rotational degrees of freedom of the particles) is reached

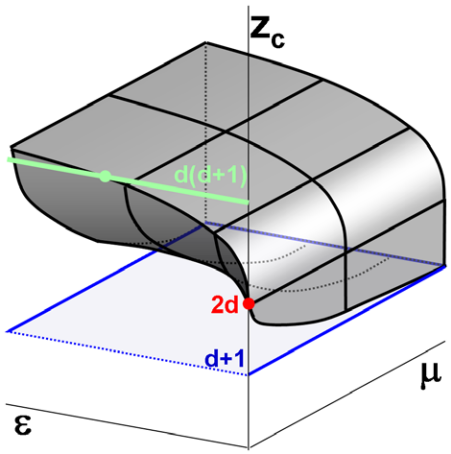

Figure 23. Conjectured range of selected contact numbers at jamming, i.e. at $P = 0$, as a function of the friction coefficient μ and ellipticity ϵ. The red dot indicates the isostatic limit for frictionless spheres at ($\mu = 0, \epsilon = 0$), the green line indicates the isostatic limit for frictionless ellipsoids ($\mu = 0, \epsilon \neq 0$) and the blue plane indicates the isostatic limit for frictional particles ($\mu \neq 0$). The contact number is precisely selected in the frictionless plane, and for sufficiently large ellipticity the contact number crosses the isostatic value (green dot). Once friction comes into play, a range of contact numbers are allowed. For a given μ and ϵ, the upper bound is given by the selected contact number for frictionless ellipsoids at $\mu = 0$, while the lower bound is given by the generalized isostaticity limit—i.e. for finite μ, the maximal number of contacts is fully mobilized here, and only for $\mu \to \infty$ does z reach the frictional isostatic value $z = d + 1$.

at the jamming threshold. The counting for ellipsoidal particles takes these rotational degrees into account, which leads to strongly hypostatic packings near jamming—however, the associated zero modes do not appear to contribute to the mechanical properties of the packings. Furthermore, the perturbation from spheres to weak ellipsoids is smooth when the trivial rotational modes for the spheres are included.

Friction, however, acts differently. Given a certain preparation procedure, the change in contact number is smooth with μ. However, the frictional interactions are such that, at the level of the dynamical matrix, the inclusion of arbitrary small friction introduces a discontinuous change. For any value of the friction the tangential stiffness takes on a finite value which leads to contributions to the dynamical matrix of order one, contributions which are absent in the frictionless case. Friction become a smooth perturbation only when the tangential stiffness is varied smoothly with μ.

6.1. Open questions

A crucial question is that of experimental relevance. Many recent predictions of the theory should be observable in experiment, in particular for frictionless systems such as foams and emulsions, but very few have been observed so far. Frictional packings have been explored theoretically far less than frictionless systems, despite their obvious experimental relevance [12, 88]. How many different order parameters

does one need to characterize the statistics of generic frictional packings?

More work is needed to clarify the notion of random loose packing [77–79] and to unravel the role of packing protocols. What is the underlying distribution of possible contact numbers and densities for frictional spheres, given a certain pressure and friction coefficient? Do RCP and RLP correspond to sharp gradients in this distribution? Are the RCP and RLP limits identical for frictionless packings? Random packings of spheres are much looser than random packings of non-spherical particles—can we understand why?

It is, in many cases, unknown how results obtained for frictionless spheres extend to more complex systems. For example, do a diverging length scale and a singularly non-affine response arise when frictional spheres or ellipses approach their isostatic limit(s)? What about the elastic moduli [71, 82]? Similarly, what is the jamming scenario for more general particles, such as frictional ellipses and nonconvex particles that may share multiple contacts? What is the scenario for more general interactions (attraction, long range, etc)?

Given the central role of the square root scaling of the contact number with distance to jamming, it would be useful to probe the connection to the square root singularity of $g(r)$—the argument outlined in section 3.4.1 assumes displacements to be primarily affine, while near J the displacements are singularly non-affine and diverge. What may happen is that the relative displacement of particles that are not in contact are not strongly non-affine—we do not know. For frictional spheres it is not understood whether $z - z_c$ exhibits true square root scaling with excess density and whether $g(r)$ exhibits similar scaling behavior there.

Essentially all the work discussed above focuses on averaged quantities and linear response. For finite systems, contact numbers, moduli, etc, exhibit significant differences in different realizations [2, 52]. Can we understand these fluctuations near jamming? What is the nonlinear yielding behavior of systems near jamming [2]?

A whole host of new phenomena arise when jammed systems are put under shear stress, and possibly are made to flow [5, 6, 8, 9], or when systems of finite temperature [10, 11] are considered. Can these phenomena be connected in a meaningful manner to the zero-shear, zero-temperature limit?

6.2. Outlook

Jamming is cool [1], as it provides a framework to approach the mechanics of disordered systems. The studies of the simplest case of static soft frictionless spheres have demonstrated that such systems exhibit rich spatial organization and anomalous mechanical properties near the isostatic/jamming limit. Important tasks for the coming years include exploring the relevance of these observations for experimental observations and for systems with more complex interactions. New horizons are emerging for systems at finite temperature and in particular for flow near jamming—as attested by the rich phenomenology of flowing foams, suspensions and granular media.

Appendix. Counting arguments for the contact number

By constraint counting one can establish bounds on the contact number [43]. First, one may require that floppy modes, deformations that in lowest non-trivial order do not cost energy, are absent. This yields a lower bound on the contact number. Packings that violate this second constraint are called hypostatic, packings that marginally fulfill this constraint are isostatic and packings that fulfill this constraint are called hyperstatic.

Note that the same lower bound on the contact number is obtained by requiring that all contact forces balance. As we will see, this is because the number of independent degrees of freedom necessary to describe changes in the energy at a contact equals the number of force degrees of freedom per contact. Therefore, the requirement that floppy modes are absent is equivalent to the requirement that the contact forces balance, and often the counting argument that yields the lower bound on z is phrased in terms of the contact forces.

Secondly, for packings at jamming, one arrives at a second constraint, which follows from the requirement that the particles are undeformed at jamming. This yields an upper bound on the contact number. Violations of this second condition are possible for special (non-generic) packings, such as perfect crystals.

As we will see, for frictionless particles the first and second bounds coincide. This does not necessarily imply that the corresponding contact numbers are *realized* at jamming: numerically it is found that frictionless spheres are indeed isostatic at jamming [2], while weakly aspherical frictionless ellipsoids are strongly hypostatic [48, 49, 59]. For frictional particles the two bounds never coincide, and numerically it is found that frictional particles are almost always hyperstatic at jamming.

Below we present the counting arguments in detail, for packings of N soft particles in d dimensions which interact through contact forces, and for which the contact number z is defined as the average number of contacts per particle. Note that the total number of contacts equals $Nz/2$—each contact is shared by two particles. As we will find below, to perform these counting arguments we need to know the number of force components per contact, or equivalently the number of independent degrees of freedom necessarily to describe changes in the energy at a contact ($\tilde{f}$), the geometrical number of degrees freedom per particle ($\tilde{x}$) and the number of force balance equations per particle ($\tilde{b}$).

Absence of floppy modes. The counting that follows from requiring that there are no floppy modes can most easily be carried out by considering ΔE, the change in elastic energy as a function of deformation of a certain packing. The number of terms contributing to ΔE equals the number of contacts, $Nz/2$, multiplied by $\tilde{f}$, the number of independent degrees of freedom necessary to describe changes in the energy at a contact. ΔE is a function of all Nd positional degrees of freedom and all additional orientational degrees of freedom which are not symmetries—zero for spheres, $2N$ for spheroids in three dimensions and $d(d-1)N/2$ for general ellipsoids.

Table A.1. Results of 'Maxwell' constraint counting for a range of different types of soft particles. As explained in the text, $\tilde{f}$ denotes the number of force components per contact, $\tilde{x}$ denotes the geometrical number of freedom per particle and $\tilde{b}$ denotes the number of balance equations per particle.

Particle	$\tilde{f}$	$\tilde{x}$	$\tilde{b}$	Touch $z/2 \leqslant \tilde{x}$	Rigidity $z\tilde{f}/2 \geqslant \tilde{b}$	Range
Frictionless sphere	1	d	d	$z \leqslant 2d$	$z \geqslant 2d$	$z = 2d$
Frictional sphere	d	d	$d(d+1)/2$	$z \leqslant 2d$	$z \geqslant d+1$	$d+1 \leqslant z \leqslant 2d$
Frictionless spheroid	1	5	5	$z \leqslant 10$	$z \geqslant 10$	$z = 10$
Frictional spheroid	3	5	6	$z \leqslant 10$	$z \geqslant 4$	$4 \leqslant z \leqslant 10$
Frictionless ellipsoid	1	$d(d+1)/2$	$d(d+1)/2$	$z \leqslant d(d+1)$	$z \geqslant d(d+1)$	$z = d(d+1)$
Frictional ellipsoid	d	$d(d+1)/2$	$d(d+1)/2$	$z \leqslant d(d+1)$	$z \geqslant d+1$	$d+1 \leqslant z \leqslant d(d+1)$

We denote these numbers of degrees of freedom relevant for ΔE by $\tilde{b}$.

Absence of generic floppy modes requires that the number of terms contributing to ΔE exceeds the number of degrees of freedom: $z\tilde{f}/2 \geqslant \tilde{b}$.

For frictionless particles, $\tilde{f}$ equals 1 because energy changes result from (de)compression of contacts only, while for frictional particles, $\tilde{f}$ equals d, since relative motions of contacting particles in all directions are relevant.

The situation for $\tilde{b}$ is simple for frictional particles, where all positional and orientational degrees of freedom are relevant and $\tilde{b} = d(d+1)/2$. For frictionless particles, $\tilde{b}$ depends on the symmetries. For frictionless spheres, only translational degrees of freedom are important and $\tilde{b} = d$. For frictionless spheroids in three dimensions, two additional rotational degrees of freedom come into play and $\tilde{b} = 5$, while for general frictionless ellipsoids all rotational degrees are relevant and $\tilde{b} = d(d+1)/2$.

Equivalence of floppy mode and force balance counting. The requirement $z\tilde{f}/2 \geqslant \tilde{b}$ is exactly the same as requiring that there are sufficient contact forces in the system so that they generically can be expected to balance: the number of contact force degrees of freedom per particles is $z\tilde{f}/2$ and the number of equations that need to be satisfied equals $\tilde{b}$. The number of relevant particle degrees of freedom in the energy expansion thus corresponds to the number of force balance equations, and the number of terms in ΔE (=number of constraints needed to generically avoid floppiness) corresponds to the number of force degrees of freedom—changes in energy and forces are directly linked.

Note that, even though the role of constraints and degrees of freedom interchanges when altering the picture between the absence of floppy modes and satisfaction of force balance, so does the requirement (floppy modes: making sure there are no generic solutions, force balance: making sure there are generic solutions), and in the force balance picture one ends up with precisely the same inequality: $z\tilde{f}/2 \geqslant \tilde{b}$.

Touch. The conditions that particles precisely touch yields $Nz/2$ constraints on the degrees of freedom of the particles. Denoting the number of geometric degrees per particle as $\tilde{x}$, the condition that for generic packings there should be less constraints than degrees of freedom yields $z/2 \leqslant \tilde{x}$.

For the particles that are considered here (spheres and ellipsoids with and without friction), the number of degrees of freedom per particles are their d positional coordinates, to which ellipsoids add their relevant angular degrees of freedom. For general ellipsoids, these yield $d(d+1)/2$ degrees of freedom—for spheroids in three dimensions (an ellipsoid with two equal axes, which thus has one symmetry of rotation—see section 5) these yield 5 degrees of freedom. The resulting counting of $\tilde{x}$ and corresponding inequalities are listed in table A.1. In particular, for frictional particles, the lower bound for the contact number is $d+1$, while for frictionless particles it depends on the symmetries of the particles.

Results. The resulting inequalities are listed in table A.1. Note that the upper bounds for z coincide for frictional and frictionless particles, as this number only depends on the geometrical number of degrees of freedom. The inequalities can be summarized as follows. For frictionless particles, $\tilde{f}$ equals 1, $\tilde{b} = \tilde{f}$ and the lower and upper bounds coincide at $z = 2\tilde{x} = 2\tilde{b}/\tilde{f}$. For frictional particles, $2\tilde{x} > 2\tilde{b}/\tilde{f}$, the lower and upper bounds do not coincide and a range of contact numbers is allowed at jamming.

References

[1] Liu A J and Nagel S R 1998 *Nature* **396** 21
[2] O'Hern C S, Silbert L E, Liu A J and Nagel S R 2003 *Phys. Rev.* E **68** 011306
[3] Lois G, Blawzdziewicz J and O'Hern C S 2008 *Phys. Rev. Lett.* **100** 028001
[4] Hastings M B, Olson Reichardt C J and Reichardt C 2003 *Phys. Rev. Lett.* **90** 098302
[5] Olsson P and Teitel S 2007 *Phys. Rev. Lett.* **99** 178001
[6] Langlois V J, Hutzler S and Weaire D 2008 *Phys. Rev.* E **78** 021401
[7] Katgert G, Mobius M E and van Hecke M 2008 *Phys. Rev. Lett.* **101** 058301
[8] Head D A 2009 *Phys. Rev. Lett.* **102** 138001
[9] Hatano T 2007 *Phys. Rev.* E **75** 060301
Hatano T 2008 *J. Phys. Soc. Japan* **77** 123002
Hatano T 2009 *Phys. Rev.* E **79** 050301
[10] Berthier L and Witten T A 2009 *Europhys. Lett.* **86** 10001
[11] Zhang Z X, Xu N, Chen D T N, Yunker P, Alsayed A M, Aptowicz K B, Habdas P, Liu A J and Nagel S R 2009 *Nature* **459** 230
[12] Majmudar T S, Sperl M, Luding S and Behringer R P 2007 *Phys. Rev. Lett.* **98** 058001
[13] Dauchot O, Marty G and Biroli G 2005 *Phys. Rev. Lett.* **95** 265701
Lechenault F, Dauchot O, Biroli G and Bouchaud J P 2008 *Europhys. Lett.* **83** 46003
[14] Keys A S, Abate A R, Glotzer S C and Durian D J 2007 *Nat. Phys.* **4** 260
Abate A R and Durian D J 2008 *Phys. Rev. Lett.* **101** 245701
[15] Bolton F and Weaire D 1990 *Phys. Rev. Lett.* **65** 3449
[16] Kraynik A M 1988 *Annu. Rev. Fluid Mech.* **20** 325

[17] Princen H M 1983 *J. Colloid Interface Sci.* **91** 160
[18] Princen H M and Kiss A D 1986 *J. Colloid Interface Sci.* **112** 427
[19] Weitz D 2004 *Science* **303** 968
[20] Makse H A, Gland N, Johnson D L and Schwartz L M 1999 *Phys. Rev. Lett.* **83** 5070
[21] Johnson D L, Makse H A, Gland N and Schwartz L 2000 *Physica* B **279** 134
[22] Makse H A, Gland N, Johnson D L and Schwartz L 2004 *Phys. Rev.* E **70** 061302
[23] Johnson K L 1985 *Contact Mechanics* (Cambridge: Cambridge University Press)
[24] Somfai E, Roux J N, Snoeijer J H, Van Hecke M and Van Saarloos W 2005 *Phys. Rev.* E **72** 1301
[25] Durian D J 1997 *Phys. Rev. Lett.* **75** 4780
Durian D J 1997 *Phys. Rev.* E **55** 1739
[26] Brakke K A 1996 *Phil. Trans. R. Soc.* A **354** 2143
http://www.susqu.edu/brakke
[27] Mason T G, Bibette J and Weitz D A 1995 *Phys. Rev. Lett.* **75** 2051
[28] Lacasse M D, Grest G S, Levine D, Mason T G and Weitz D A 1996 *Phys. Rev. Lett.* **76** 3448
[29] Mason T G, Lacasse M D, Grest G S, Levine D, Bibette J and Weitz D A 1997 *Phys. Rev.* E **56** 3150
[30] Ellenbroek W G, Somfai E, van Hecke M and van Saarloos W 2006 *Phys. Rev. Lett.* **97** 258001
[31] Ellenbroek W G, van Hecke M and van Saarloos W 2009 arXiv:0911.0944
[32] Radjai F and Roux S 2002 *Phys. Rev. Lett.* **89** 064302
[33] Tanguy A, Wittmer J P, Leonforte F and Barrat J L 2002 *Phys. Rev.* B **66** 4205
[34] Tanguy A, Leonforte F, Wittmer J P and Barrat J L 2004 *Appl. Surf. Sci.* **226** 282
[35] Lemaître A and Maloney C 2006 *J. Stat. Phys.* **123** 415
[36] Maloney C E 2006 *Phys. Rev. Lett.* **97** 035503
[37] Kasahara A and Nakanishi H 2004 *Phys. Rev.* E **70** 051309
[38] Donev A, Torquato S, Stillinger F H and Connelly R 2004 *Phys. Rev.* E **70** 043301
O'Hern C S, Silbert L E, Liu A J and Nagel S R 2004 *Phys. Rev.* E **70** 043302
[39] Press W H, Flannery B P, Teukolsky S A and Vetterling W T 1986 *Numerical Recipes in Fortran 77* (New York: Cambridge University Press)
[40] O'Hern C S, Langer S A, Liu A J and Nagel S R 2002 *Phys. Rev. Lett.* **88** 075507
[41] Torquato S, Truskett T M and Debenedetti P G 2000 *Phys. Rev. Lett.* **84** 2064
[42] Silbert L E, Liu A J and Nagel S R 2006 *Phys. Rev.* E **73** 041304
[43] Alexander S 1998 *Phys. Rep.* **296** 65
[44] Moukarzel C F 1998 *Phys. Rev. Lett.* **81** 1634
[45] Tkachenko A V and Witten T A 1999 *Phys. Rev.* E **60** 687
[46] Silbert L E, Ertaş D, Grest G S, Halsey T C and Levine D 2002 *Phys. Rev.* E **65** 031304
[47] Donev A, Torquato S and Stillinger F H 2005 *Phys. Rev.* E **71** 011105
[48] Donev A, Connelly R, Stillinger F H and Torquato S 2007 *Phys. Rev.* E **75** 051304
[49] Mailman M, Schreck C F, O'Hern C S and Chakraborty B 2009 *Phys. Rev. Lett.* **102** 255501
[50] Zeravcic Z, Xu N, Liu A J, Nagel S R and van Saarloos W 2009 *Europhys. Lett.* **87** 26001
[51] Ellenbroek W and Zeravcic Z 2008 private communication
[52] Henkes S and Chakraborty B 2009 *Phys. Rev.* E **79** 061301
[53] Henkes S, van Hecke M and van Saarloos W 2009 arXiv:0907.3451
[54] Wyart M, Silbert L E, Nagel S R and Witten T A 2005 *Phys. Rev.* E **72** 051306
Wyart M 2005 *Ann. Phys. Fr.* **30** 1
Wyart M, Nagel S R and Witten T A 2005 *Europhys. Lett.* **72** 486
[55] Tkachenko A V and Witten T A 2000 *Phys. Rev.* E **62** 2510
[56] Silbert L E, Liu A J and Nagel S R 2005 *Phys. Rev. Lett.* **95** 098301
[57] Leonforte F, Tanguy A, Wittmer J P and Barrat J L 2004 *Phys. Rev.* B **70** 014203
[58] Silbert L E, Liu A J and Nagel S R 2009 *Phys. Rev.* E **79** 021308
[59] Zeravcic Z, van Saarloos W and Nelson D 2008 *Europhys. Lett.* **83** 44001
[60] Xu N, Vitelli V, Liu A J and Nagel S R 2009 arXiv:0909.3701
[61] Goldenberg C and Goldhirsch I 2002 *Phys. Rev. Lett.* **89** 084302
Goldenberg C and Goldhirsch I 2005 *Nature* **435** 188
[62] Ellenbroek W G, Zeravcic Z, van Saarloos W and van Hecke M 2009 *Europhys. Lett.* **87** 34004
[63] Wyart M, Liang H, Kabla A and Mahadevan L 2008 *Phys. Rev. Lett.* **101** 215501
[64] Feng S and Sen P N 1984 *Phys. Rev. Lett.* **52** 216
[65] Feng S, Thorpe M F and Garboczi E 1985 *Phys. Rev.* B **31** 276
[66] Jacobs D J and Thorpe M F 1995 *Phys. Rev. Lett.* **75** 4051
Moukarzel C and Duxbury P M 1995 *Phys. Rev. Lett.* **75** 4055
[67] Makse H A, Johnson D L and Schwartz L M 2000 *Phys. Rev. Lett.* **84** 4160
[68] Unger T, Kertesz J and Wolf D E 2005 *Phys. Rev. Lett.* **94** 178001
[69] Zhang H P and Makse H A 2005 *Phys. Rev.* E **72** 011301
[70] Shundyak K, van Hecke M and van Saarloos W 2007 *Phys. Rev.* E **75** 010301
[71] Somfai E, van Hecke M, Ellenbroek W G, Shundyak K and van Saarloos W 2007 *Phys. Rev.* E **75** 020301(R)
[72] Halsey T C and Ertas D 1999 *Phys. Rev. Lett.* **83** 5007
[73] Silbert L E 2008 *Jamming of frictional spheres and random loose packing* preprint and Private Communication
[74] Johnson K L 1985 *Contact Mechanics* (Cambridge: Cambridge University Press)
[75] Somfai E, van Hecke M, Ellenbroek W G, Shundyak K and van Saarloos W 2005 arXiv:0510506v1
[76] Knight J B, Fandrich C G, Lau C N, Jaeger H M and Nagel S R 1995 *Phys. Rev.* E **51** 3957
Ben-Naim E, Knight J B, Nowak E R, Jaeger H M and Nagel S R 1998 *Physica* D **123** 380
Richard P, Nicodemi M, Delanney R, Ribiere P and Bideau D 2005 *Nat. Mater.* **4** 121
[77] Onoda G Y and Liniger E G 1990 *Phys. Rev. Lett.* **64** 2727
[78] Song C, Wang P and Makse H A 2008 *Nature* **453** 629
[79] Ciamarra M P and Coniglio A 2008 *Phys. Rev. Lett.* **101** 128001
[80] Bernal J D and Mason J 1960 *Nature* **188** 910
Scott G D 1960 *Nature* **188** 908
Finney J L 1970 *Proc. R. Soc.* A **319** 479
Berryman J G 1983 *Phys. Rev.* A **27** 1053
[81] Bouchaud J-P 2004 *Proc. Les Houches Summer School of Theoretical Physics* (*Session LXXVII*) ed J-L Barrat, M Feigelman, J Kurchan and J Dalibard
[82] Magnanimo V, La Ragione L, Jenkins J T, Wang P and Makse H A 2008 *Europhys. Lett.* **81** 34006
[83] Donev A, Cisse I, Sachs D, Variano E A, Stillinger F H, Connelly R, Torquato S and Chaikin P M 2004 *Science* **303** 990
[84] Philipse A P 1996 *Langmuir* **12** 1127
Philipse A P 1996 *Langmuir* **12** 5971 (correction)
[85] Williams S R and Philipse A P 2003 *Phys. Rev.* E **67** 051301
[86] Philipse A P, private communication
[87] Donev A, Stillinger F H, Chaikin P M and Torquato S 2004 *Phys. Rev. Lett.* **92** 255506
[88] Jacob X, Aleshin V, Tournat V, Leclaire P, Lauriks W and Gusev V E 2008 *Phys. Rev. Lett.* **100** 158003
Bonneau L, Andreotti B and Clement E 2008 *Phys. Rev. Lett.* **101** 118001